University of Alberta

Library Release Form

NAME OF AUTHOR:	Farhana Sobratee
TITLE OF THESIS:	M11 Channel at TRIUMF, Another Surface Muon Source
DEGREE:	Master of Science
YEAR THIS DEGREE GRANTED:	2000

Farhana Sobratee
Apartment 1007
11147 82 Avenue
Edmonton Alberta T6G 0T5
CANADA

December 23, 1999

You will never be happy if you continue to search for what happiness consists of. You will never live if you are looking for the meaning of life.

Albert Camus

University of Alberta

M11 Channel at TRIUMF, Another Surface Muon Source

by

Farhana Sobratee

A thesis submitted to the Faculty of Graduate Studies and Research in partial fulfillment of the requirements for the degree of Master of Science

Department of Physics

Edmonton, Alberta

Spring 2000

University of Alberta

Faculty of Graduate Studies and Research

The undersigned certify that they have read, and recommend to the Faculty of Graduate Studies and Research for acceptance, a thesis entitled **M11 Channel at TRIUMF, Another Surface Muon Source** submitted by **Farhana Sobratee** in partial fulfillment of the requirements for the degree of Master of Science.

Nathan L. Rodning (Supervisor)

Michael Brett (External)

W. John McDonald

Helmy S. Sherif

DATE:

To

Missrah, my mother.

Abstract

This thesis presents the results of a beam test on the M11 channel at TRIUMF using data collected with a Muon Spin Rotation (μSR) detector setup. The beam test was performed at a momentum range of few percent above and below the $\mu - \pi$ edge (at 29.79 Mev/c) to search for polarized muons. The polarized muons (a.k.a. surface muons) are produced from a π^+ decay at rest near the surface of the production target. Some interesting features of the surface and unpolarized cloud muons in the beam are presented at this momentum range. The background and its depolarization effect on the surface muons across the cyclotron RF period of 43.6 ns are investigated. It was found that this beamline can be used as a surface μ^+ source.

Acknowledgements

I would like to thank Professor Nathan L. Rodning of the University of Alberta for his guidance, support and time, and for being my supervisor since April 1998. The funding from the Research Corporation for one semester is gratefully acknowleged. I appreciate the contribution of all the people of the E614 collaboration and the people of the μSR facility at TRIUMF for making this beam test possible. Also my sincere acknowledgement goes to Dr Peter W Green for his patience in helping me out with using his NOVA data analysis system.

The members of the supervisory and examining committee and specially the E614 collaborators, Dr David Gill, Dr Pierre Depommier, Dr Carl Gigliardi and Dr Peter Gumplinger have my gratitude for their many useful comments.

Finally, I would like to thank all of my friends and colleagues for their support.

Table of Contents

List of Tables

List of Figures

Chapter 1

INTRODUCTION

1.1 Motivation and Objectives

It was suggested that the M11 channel can be an alternative source of polarized muons at TRIUMF for various muon stopping experiments and that it can be used to perform preliminary diagnostic tests for experiment E614. E614 is a high precision muon decay experiment under preparation at TRIUMF and will be performed on the M13 beamline.

The objective of the beam test on M11 is to search for polarized muons. M11 is a secondary beamline optimized for the transport of high momentum pions and muons, and had not been used previously at low momentum. The polarized muons on the M11 beamline are "surface" muons which are produced from pions decaying at rest at the surface of the production target. The physics behind the production of the ideal monoenergetic polarized muons is given in Chapter 2.

On seeing the signature time of flight spectra of polarized muons during a preliminary test with a simple set-up of three scintillators, arrangement was made for an experimental set-up whereby a technique called muon spin rotation (μSR) is used. From this the following quantities are determined for M11:

- the flux of the different particles in the beamline (polarized and unpolarized muons, positrons and pions),
- the polarization of the muons,
- and a time window to discriminate between polarized muons and contaminant particles.

An overview of the μSR technique which involves the stopping and decay of a polarized muon will be provided in Chapter 2. Chapter 3 will elaborate on the experimental set-up. The analysis of the data and results will be discussed in Chapter 4, and finally the conclusion will be given Chapter 5.

Chapter 2

THEORY

2.1 The ideal monoenergetic polarized μ beam

The collision of an accelerated primary proton beam ($\sim$ 500 MeV) with the nuclei of the production target, e.g. carbon ^{12}C, produces positive pions (π^+) via the possible reaction

$$p +^{12} C \rightarrow \pi^+ + X.$$

From the subsequent decay of the pions (τ_{π^+}=26.03 ns), positive muons (μ^+) are formed via the two-body decay

$$\pi^+ \rightarrow \mu^+ + \nu_\mu.$$

In the pion's rest frame, linear momentum conservation requires that the decay products, μ^+ and ν_μ are emitted in opposite directions with equal momenta. Also because the pion is a spinless particle (i.e. it has no intrinsic angular momentum), conservation of angular momentum requires that μ^+ and ν_μ have equal and opposite spin. This decay process is governed by the weak interaction which - as defined in the Standard Model - has the remarkable property that it creates only left-handed or negative helicity neutrinos, i.e. the neutrinos have their

	positive muon μ^+	**positive pion** π^+	**positron** e^+
Lifetime	2.19703(4) μs	26.033(5) ns	$>4.3\times10^{23}$ y
Type	lepton	meson	lepton
Mass (MeV/c^2)	105.658389(34)	139.56995(35)	0.51099907(15)
Mass (m_e)	207	273	1
Charge (e)	+1	+1	+1
Spin ($\hbar$)	$\frac{1}{2}$	0	$\frac{1}{2}$

Table 2.1: Selected properties of the positive muon and other particles [1].

	electron neutrino ν_e	**muon neutrino** ν_μ
Type	lepton	lepton
Mass	$<$ 15 eV	$<$ 0.17 MeV
Mean life/mass	$>$ 7 $\times10^9$ s/eV	$>$ 15.4 s/eV
Charge (e)	0	0
Spin ($\hbar$)	$\frac{1}{2}$	$\frac{1}{2}$

Table 2.2: Selected properties of the electron and muon neutrinos [1].

spin angular momentum and linear momentum in opposite direction; and right-handed or positive helicity antineutrinos. The mirror-image reaction does not occur in nature, because the parity inversion performed by the mirror changes a left-handed neutrino to a right-handed one, which the weak interaction has not been seen to produce. Hence, the μ^+ must also have its spin antiparallel to its momentum. This gives a monoenergetic beam of perfectly spin-polarized muons from pion decay. Some properties of the positive muon and other particles referred to in this thesis are given in Table 2.1 and Table 2.2.

2.2 The Surface Muon Beam

The surface muon beam also known as "Arizona" beam was first realized after the pioneering work of Pifer *et al.* in 1976 from University of Arizona [2]. The concept of surface muon beams was motivated by the search for muonium-to-antimuonium conversion $\mu^+e^- \to \mu^-e^+$ [3]. It arose because of the need for high intensities of low energy μ^+'s that can be stopped in samples of convenient thickness (less than 1 cm). These are available in the required intensities only from the two-body pion decay

$$\pi^+ \to \mu^+ + \nu_\mu, \tag{2.1}$$

from which the muon emerges with a momentum of 29.79 MeV/c and a kinetic energy of 4.119 MeV in the pion rest frame. The lifetime of the free charged pion is 26.03 ns.

Commonly, μ^+ beams today are emitted from pion decay at rest in the surface layer of the primary target where the pions themselves are produced by collisions of high energy protons with the target nuclei, as illustrated in Figure 2.1 - hence the common name, *surface muons* [3]. This mode is not available for negative muons because a negative pion (π^-) stopping in the target behaves like a heavy electron and rapidly cascades down to tightly bound orbitals where the π^- wavefunction overlaps with the nuclear wave function resulting in a very high probability for strong interactions. Positive pions that have come to rest in solids take up interstitial positions between atoms so they are too far from nuclei to be captured. Their lifetime is unaffected by any properties of the target material.

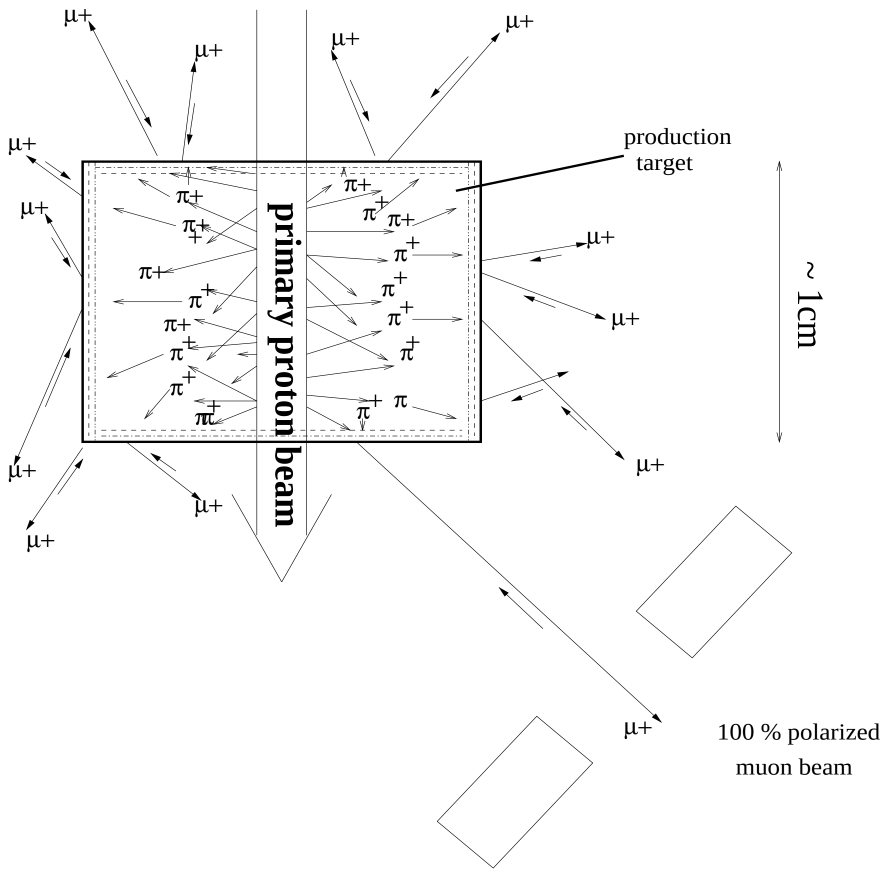

Figure 2.1: "Arizona" or "surface muon" beam produced from pion decaying at rest near the surface of the production target.

2.2.1 Surface Muon As A Probe

An ever-increasing number of stopping muon (μ^+) experiments involve sub-atomic, atomic, molecular and condensed-matter physics and chemistry. The most rapidly expanding application of surface muon beams is the muon spin rotation and/or relaxation (μSR), where muons probe a variety of states of matter. In these applications, the surface muon beam offers the advantages of high stopping rates in very small samples, a high degree of polarization and low cost of construction and operation [3].

In the chemical application, simple calculations of chemical reaction processes and molecular structure are allowed due to the fact that the muonium atom ($Mu=\mu^+e^-$) and the hydrogen atom have the same size, almost the same reduced mass and ionizing potential.

The application in condensed matter physics might be titled: "The Muon as a Magnetic Probe." Here μ^+SR is used to learn the location, electronic structure and dynamical behaviour of muonium atoms in semiconductors. The study of quantum diffusion of μ^+ and Mu in solids is another very important field, having implications for the electronic and diffusive transport properties of the material. Because muon decay provides a non-electromagnetic "signal," μSR is a unique probe for the magnetic behaviour of superconductors without causing distortion.

In particle physics the surface muon makes possible the study of the main muon decay mode $\mu \to e\nu\bar{\nu}$ which serves as an ideal probe of the space-time structure of the weak interaction. This comes about because the purely leptonic nature of this decay eliminates any uncertainties due to the internal structure of the particles.

2.3 Parity Violation

It was proposed by Lee and Yang in 1956 [4] that space-time principles of invariance under charge conjugation, time reversal, and parity transformation are violated by the weak interactions responsible for the decay of nuclei, mesons, and strange particles. Their hypothesis was accompanied by the suggestion that confirmation should be sought (among other places) in the study of the successive decay reactions

$$\pi^+ \to \mu^+ \, \nu_\mu \tag{2.2}$$

$$\mu^+ \to e^+ \, \bar{\nu}_\mu \, \nu_e \; . \tag{2.3}$$

They pointed out that parity nonconservation implies a polarization of the spin of the antimuons (μ^+'s) emitted from stopped pions (π^+'s) in Equation (2.2) opposite the direction of motion and that furthermore, the angular distribution of the positrons e^+ in Equation (2.3) should serve as an analyzer for the muon polarization. The first confirmation of parity violation in weak interactions immediately followed from the results of

- the famous experiment on β decay of oriented nuclei by Wu *et al.* [5],
- and the above suggested meson experiment performed by Garwin *et al.*, by stopping, in carbon, the μ^+ beam formed by forward decay in flight of π^+ mesons [6].

The most remarkable feature of the positive pion decay is that it maximally violates parity symmetry, causing the μ^+ to be emitted with perfect spin polarization (Figure 2.2). The propensity of the muon decay positron in (2.3) to be emitted in the direction of the spin of the μ^+ is another consequence of parity violation which allows us to infer the muon spin distribution. The information is delivered to the experimenter in the form of rather high energy (up to 52.83 MeV) positrons which readily penetrate sample holders, cryostat and the detectors used to establish the time and direction of the muon decay.

2.4 Michel Spectrum- the Standard Model explanation for muon decay

Soon after the discovery of parity violation it was established that to the first approximation the weak charged currents have "$V - A$" (vector minus axial vector) structure. All measurements in direct muon decay $\mu^- \rightarrow e^- + \nu_\mu + \overline{\nu}_e$, and its inverse, $\nu_\mu + e^- \rightarrow \mu^- + \nu_e$ are successfully described by the "V-A"

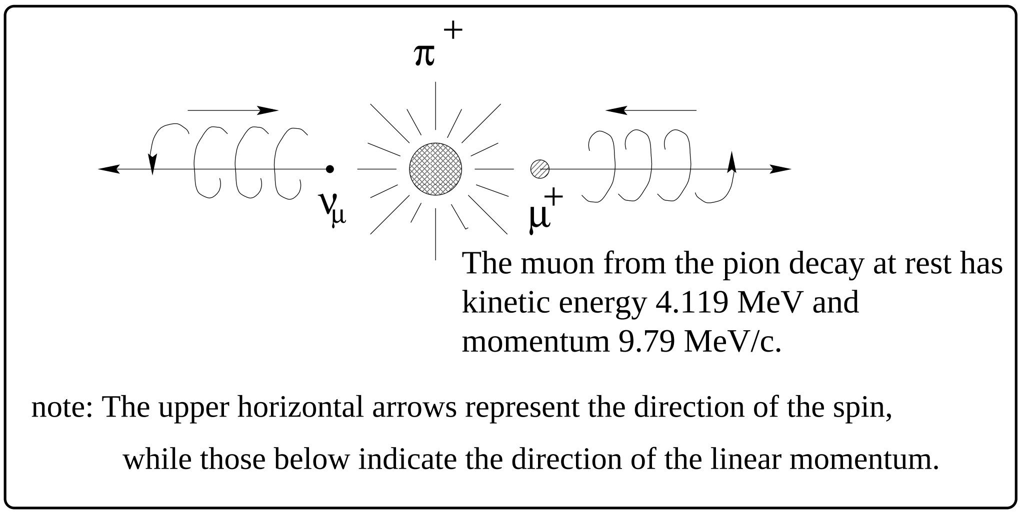

Figure 2.2: A pion π^+ decay at rest (the mirror image of which can not occur in nature) producing a perfectly polarized antimuon μ^+ and neutrino ν_μ.

interaction, which is a particular case of a local, derivative-free, lepton-number conserving, four fermion interaction [7]. At energies well below $m_W c^2$, where m_W $(= 80.41 \pm 0.10$ GeV) is the mass of W, the intermediate vector boson mediating the weak interaction, the matrix element of muon decay is

$$\sum_{\substack{\gamma=S,V,T \\ \epsilon,\mu=R,L}} g^{\gamma}_{\epsilon\mu} \langle \bar{e}_\epsilon | \Gamma^\gamma | \nu_e \rangle \langle \bar{\nu}_\mu | \Gamma_\gamma | \mu_\mu \rangle. \tag{2.4}$$

γ labels the type of interaction: Γ^S, Γ^V, Γ^T represent a scalar, vector, or tensor interaction. The indices $\epsilon, \mu = R, L$ indicate the right- or left-handed chirality of the electron or muon. The chiralities of the states ν_e and $\bar{\nu}_\mu$ are then determined by the values of γ, ϵ and μ. Existing information on the weak coupling constants, $g^{\gamma}_{\epsilon\mu}$ are given in Table 2.3.

The muon decay mode $\mu \to e\nu\bar{\nu}$ has a branching ratio of $\approx 100\%$ [1]. Table 2.4 below shows the information on the μ^+ decay modes.

$\mid g^S_{RR} \mid < 0.066$	$\mid g^V_{RR} \mid < 0.033$	$\mid g^T_{RR} \mid \equiv 0$
$\mid g^S_{LR} \mid < 0.125$	$\mid g^V_{LR} \mid < 0.060$	$\mid g^T_{LR} \mid < 0.036$
$\mid g^S_{RL} \mid < 0.424$	$\mid g^V_{RL} \mid < 0.110$	$\mid g^T_{RL} \mid < 0.122$
$\mid g^S_{LL} \mid < 0.550$	$\mid g^V_{LL} \mid > 0.960$	$\mid g^T_{LL} \mid \equiv 0$

Table 2.3: Coupling constants $g^{\gamma}_{\epsilon\mu}$. 90% confidence level experimental limits [[1]]. The experimental uncertainty on the muon polarization in pion decay is included

.

Neglecting radiative corrections and masses of the neutrinos and $e^{\pm}$, the differential decay probability to obtain an $e^{\pm}$ with (reduced) energy between x and $x + dx$, emitted at an angle between θ and $\theta + d\theta$ with respect to the muon spin $\vec{P}_\mu$ in the rest frame of a muon ($\mu^{\pm}$) measured by a polarization insensitive detector, is given by

$$\frac{d^2\Gamma}{x^2 dx\ d\cos\theta} \sim 3(1-x) + \frac{2\rho}{3}(4x-3) \pm P_\mu \xi \cos\theta \left[1 - x + \frac{2\delta}{3}(4x-3)\right]. \tag{2.5}$$

$P_\mu = |\vec{P}_\mu|$ is the degree of muon polarization and $x \equiv E_e/\max(E_e)$ is the reduced energy, where the maximum $e^{\pm}$ energy, $\max(E_e) = m_\mu/2 = 52.83$ MeV. ρ, ξ, and δ and another parameter η, that appears if m_e is not neglected, are the Michel parameters which are bilinear combinations of the weak interaction coupling constants $g^{\gamma}_{\epsilon\mu}$. The Standard Model interaction corresponds to one single amplitude g^V_{LL} being unity and all the others being zero, which gives $\rho = \xi\delta = 3/4$, $\xi = 1$ and $\eta = 0$.

μ^+ **Decay Modes**		
Mode	**fraction** $(\Gamma_l\Gamma)$	**Confidence level**
Γ_1 $e^+\bar{\nu_\mu}\nu_e$	$\approx 100\%$	
Γ_2 $e^+\bar{\nu_\mu}\nu_e\gamma$	$(1.4\pm0.4)\%$	
Γ_3 $e^+\bar{\nu_\mu}\nu_e e^+e^-$	$(3.4 \pm 0.4) \times 10^-5$	
Γ_4 $e^+\nu_\mu\bar{\nu_e}$	$< 1.2\%$	90%
Γ_5 $e^+\gamma$	$< 1.2 \times 10^-11$	90%
Γ_6 $e^+e^-e^+$	$< 1.0 \times 10^{-12}$	90%
Γ_7 $e^+2\gamma$	$< 7.2 \times 10^{-11}$	90%

Table 2.4: Experimental data on muon decay modes [1]. The limit on Γ_5 was updated in 1999 [8].

2.4.1 The asymmetry, α

The energy and angular distribution of $e^\pm$ from $\mu^\pm$ decay, Equation (2.5), can be rewritten as

$$\frac{d^2\Gamma}{dx\ d\cos\theta} \sim F(x)\ \left[1 + \alpha(x)\cos\theta\right], \tag{2.6}$$

where $\alpha(x)$ is the anisotropic part of the spectrum, traditionally called the asymmetry and also connotes the *polarization of the muon spin ensemble* since it incorporates P_μ; and $F(x)$ is the isotropic energy dependent term. Using the Standard Model value of the Michel parameters, the asymmetry factor α depends on the $e^\pm$ energy as

$$\alpha(x) = \pm P_\mu \frac{2x-1}{3-2x}$$

and the normalized isotropic part of $e^\pm$ energy spectrum has the form

$$F(x) = 2x^2(3-2x)$$

The decay distribution (Equation 2.6), $F(x)$ and $\alpha(x)$ are shown graphically in Figure 2.3.

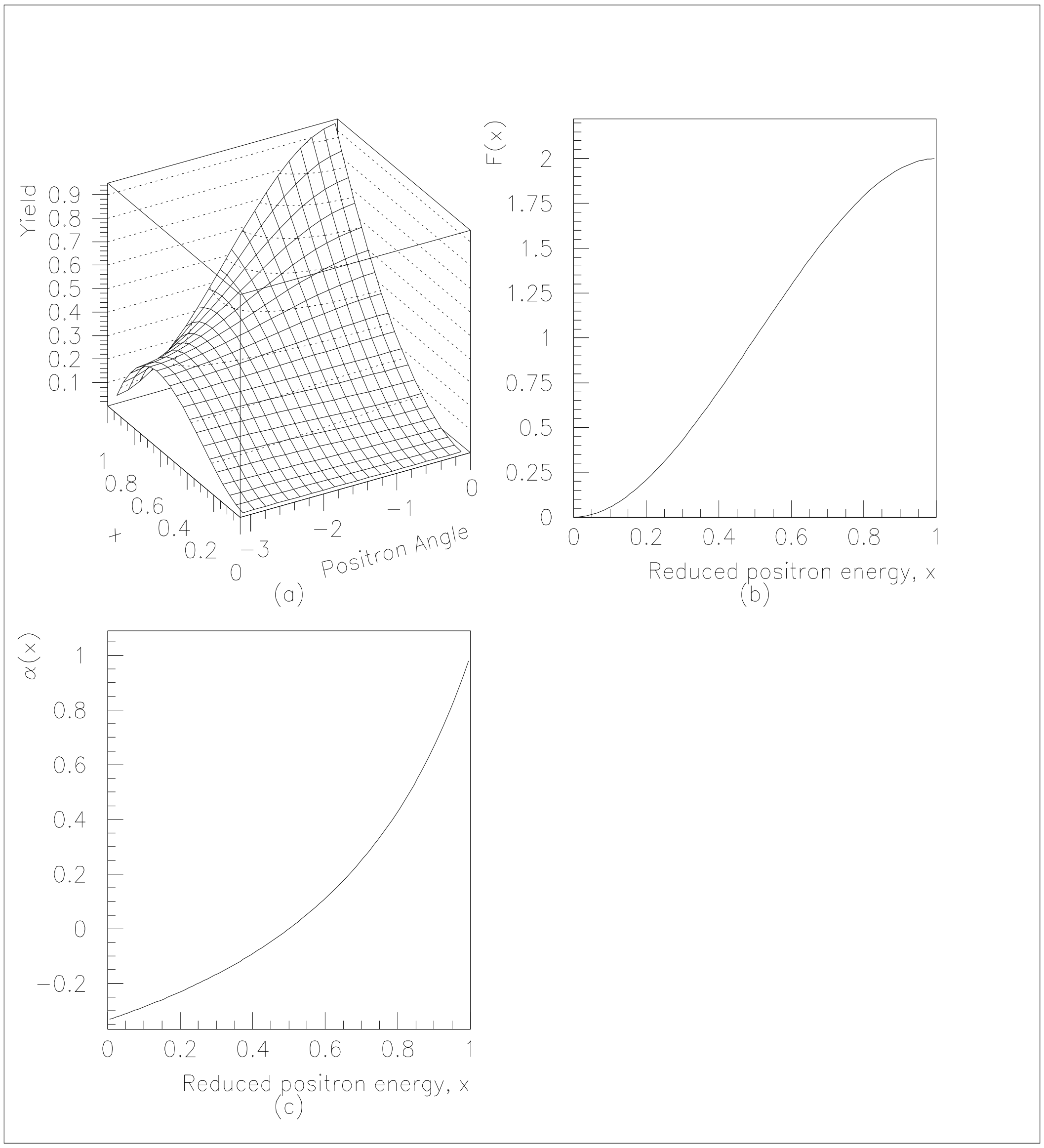

Figure 2.3: Reduced e^+ energy dependence of:(a) the energy and angular distribution of e^+ from μ^+ decay, (b) the isotropic energy term, $F(x)$ in the Michel spectrum, and (c) μ^+ decay asymmetry $\alpha(x)$.

For a 100% polarized $\mu^{\pm}$ beam, the theoretical asymmetry averaged over all the possible $e^{\pm}$ energies from $x = 0$ to $x = 1$ is

$$\langle \alpha \rangle = \int_0^1 \alpha(x)\ F(x)\ dx = \pm\frac{1}{3},$$

which is very difficult to realize in practice. The empirical asymmetry α in a given detector is dependent on the thickness, geometry and material of detectors and target and the magnetic field.

2.5 Muon Spin Rotation, μSR

The beam test makes use of the μSR techniques whereby interesting properties of the M11 channel are found. An overview of the physics taking place in μSR is given here. The success of the μSR technique relies on two circumstances. These are: the intrinsic polarization of the muons during their production from pions $\pi^+ \to \mu^+\nu$; and the anisotropy (preferred direction along the muon spin) of the positron emission in their subsequent decay $\mu^+ \to e^+\bar{\nu_\mu}\nu_e$ [10].

In this beam test the μSR technique is used to measure the polarization of the surface muon beam. The muons are actually stopped in the sample in an external magnetic field and decay at rest into a positron, a neutrino and antineutrino (Figure 2.4). Muon spin rotation is illustrated in schematic form in Figure 2.5. It is worthwhile to mention that it is not a scattering process. The essence of muon spin rotation lies in the fact that the magnetic field applied transverse (perpendicular) to the initial direction of the muon spin polarization vector causes the the muon spin to precess around it at its Larmor frequency (Figure 2.5(b)), given by the muon gyromagnetic ratio

$$\gamma_\mu/2\pi = \frac{1}{2\pi}\frac{e[C]}{m_\mu[kg]} = 1.3553879(9) \times 10^8\ \mathrm{Hz}\ \mathrm{T}^{-1}.$$

The incident surface muon beam produced in the pion decay process is essentially

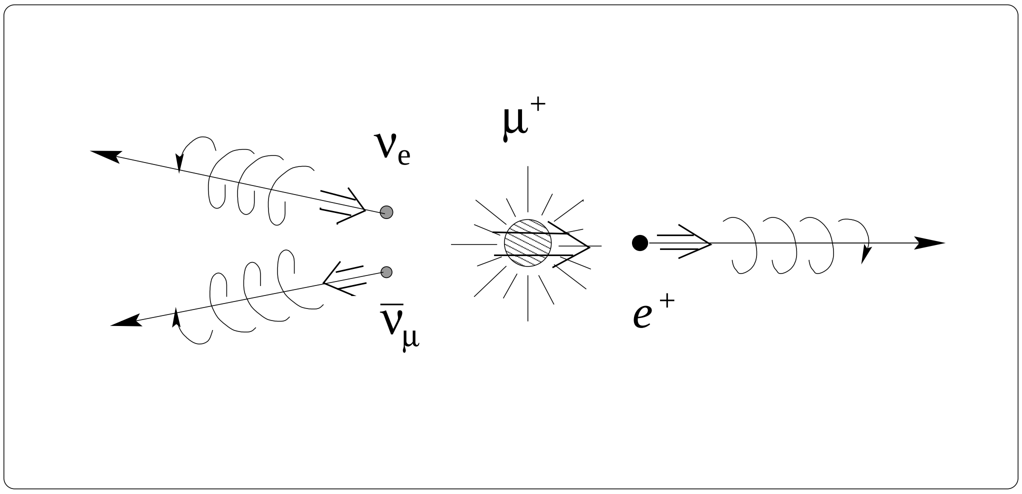

Figure 2.4: Schematic form of positive muon decay in the maximum probability case when the neutrino and antineutrino go off in the same direction together, and the positron exits along the antimuon's spin with maximum energy of 53 MeV.

100% polarized. The initial polarization of the muon can be substantially preserved throughout the transport of the beam (in part because $g_\mu - 2$ is small) and in the actual process of implantation and thermalization. On implantation into matter all muon spins point in the same direction and in the absence of other interactions will decay with a characteristic angular distribution $P(\theta) = 1 + \alpha\cos(\theta)$ (Figure 2.6), favouring the direction of the polarization vector.

Information on the muon polarization is carried by the decay positrons which are sufficiently energetic to escape from the sample and are readily detected in simple scintillation counters placed in the plane which is along the beam direction, perpendicular to the magnetic field. One can imagine a somewhat diffuse 'lighthouse beam' of positrons sweeping around, periodically illuminating the detector.

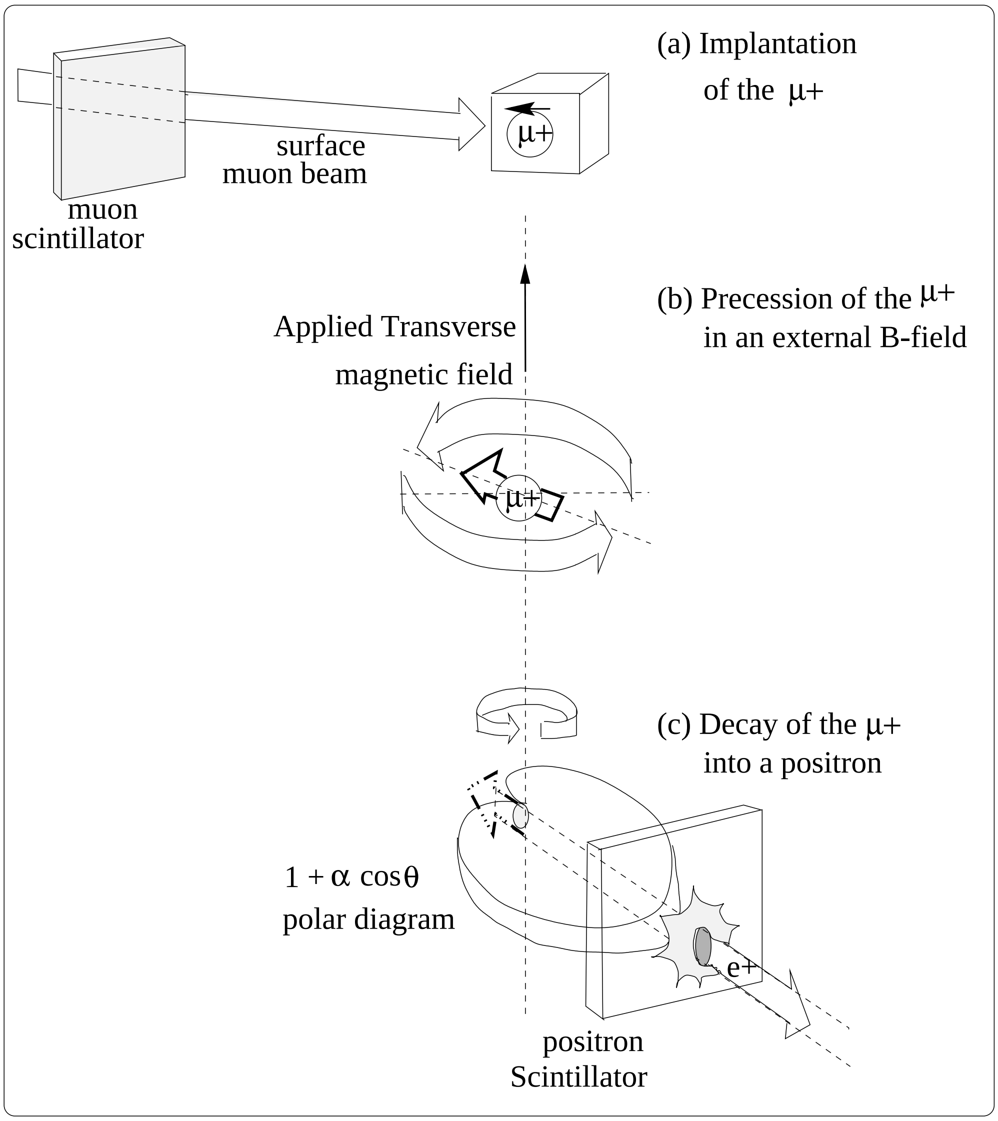

Figure 2.5: Representation of (a) muon implantation (b) muon spin rotation (i.e. Larmor precession in a transverse magnetic field) and (c) disintegration of the muons and detection of the emitted positrons. The polar diagram in (c) rotates with the muon spin.

Decay event data from the positron scintillation counters are fed into an electronic data acquisition system leading to the gradual accumulation of a muon spin rotation spectrum of decay event counts against time, an example of which is shown in Figure 2.7. The horizontal axis represents the time elapsed from the detection of a muon in the muon counter to its decay into a positron in the sample. The overall exponential decay reflects the muon lifetime (2.2 microseconds) and the precession of the muon spins is manifest in the superimposed oscillations as the muon polarization sweeps past the positron detector.

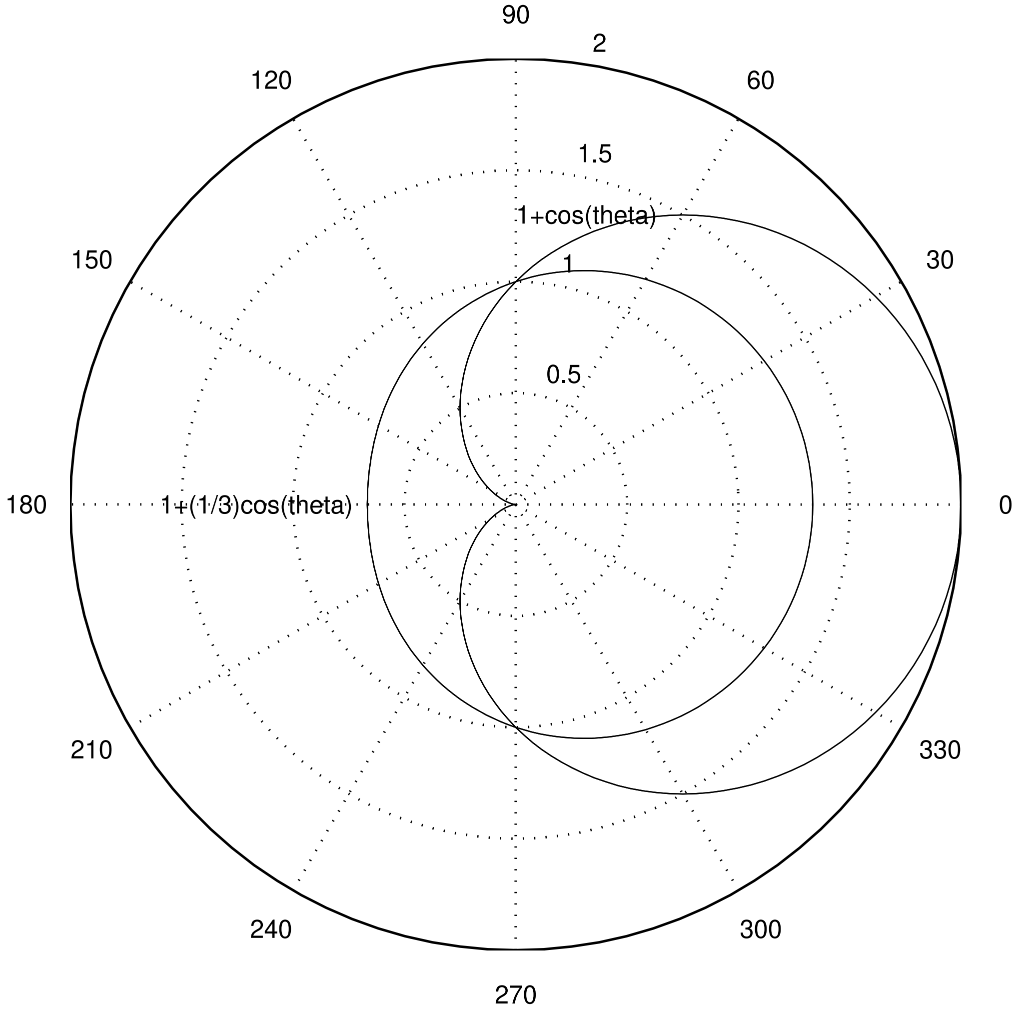

Figure 2.6: Angular distribution $P(\theta) = 1 + \alpha\cos(\theta)$ of the e^+ from μ^+ decay. The asymmetry (anisotropy) α is 100% for the highest e^+ energy (52.83 MeV) and $\frac{1}{3}$ when averaged over all possible e^+ energies.

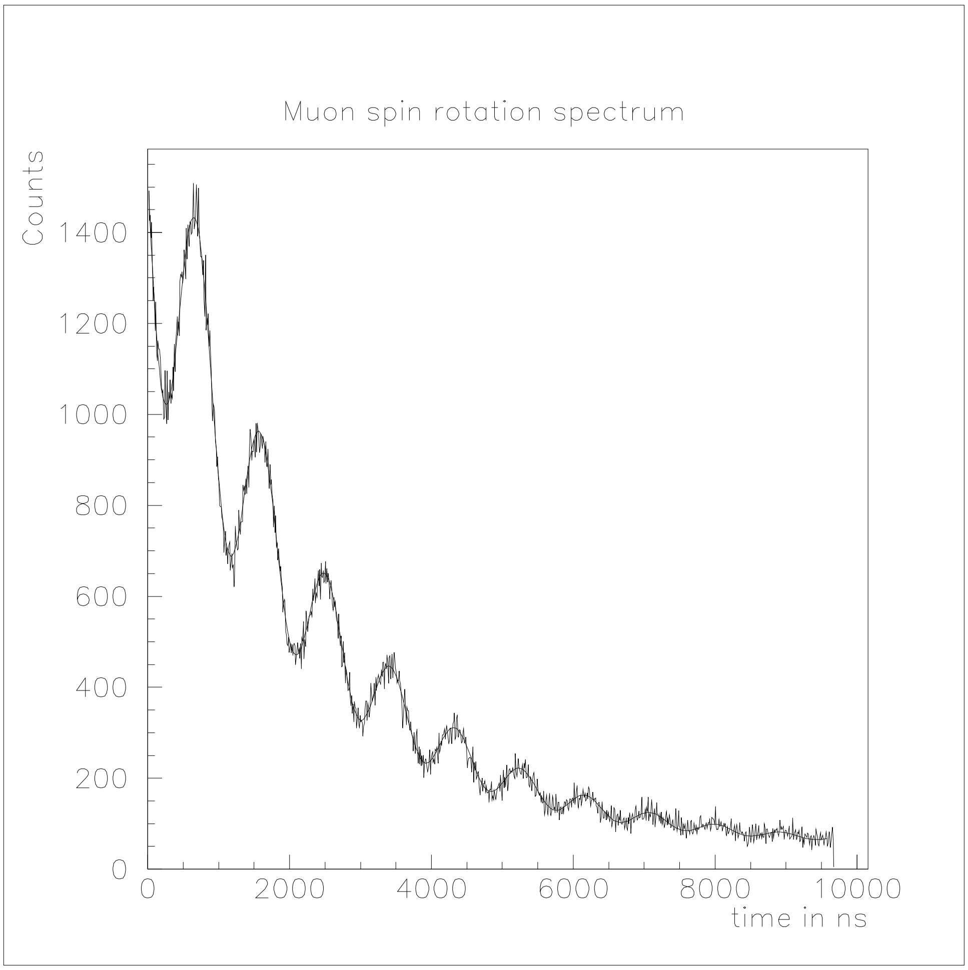

Figure 2.7: Time spectrum for a simple μSR experiment with a transverse field.

Chapter 3

EXPERIMENTAL SET-UP

3.1 M11 Secondary Beamline

The experiment was performed on one of the secondary beamlines, M11, of the 500-MeV cyclotron at TRIUMF, Vancouver (Figure 3.1). The cyclotron has a beam burst period of 43.6 ns so that a brief pulse ($\sim$ 4 ns) of protons is delivered every 43.6 ns (at high currents it is necessary to spread the proton beam pulse out in time to reduce space charge effects). M11 views the production target 1AT1 which is 1 cm graphite at $\approx 3^o$ with respect to the primary proton beam, and can be tuned to select surface muons obtained from the decay of positive pions (π^+). The pions are first produced by the collision of the primary proton beam with the nuclei of the 1AT1 target. Positive pions then decay with a lifetime of 26.03 ns to produce one muon neutrino (ν_μ) and one positive muon (μ^+).

Perhaps the most important development in muon beam technology was the realization that by removing the windows that isolated the primary and secondary particle beamlines, and turning down the momentum tuning of the secondary channel, the low momentum positively charged surface muons could be brought out to an experiment [2]. Those positive pions that happen to come to

Figure 3.1: TRIUMF beamlines

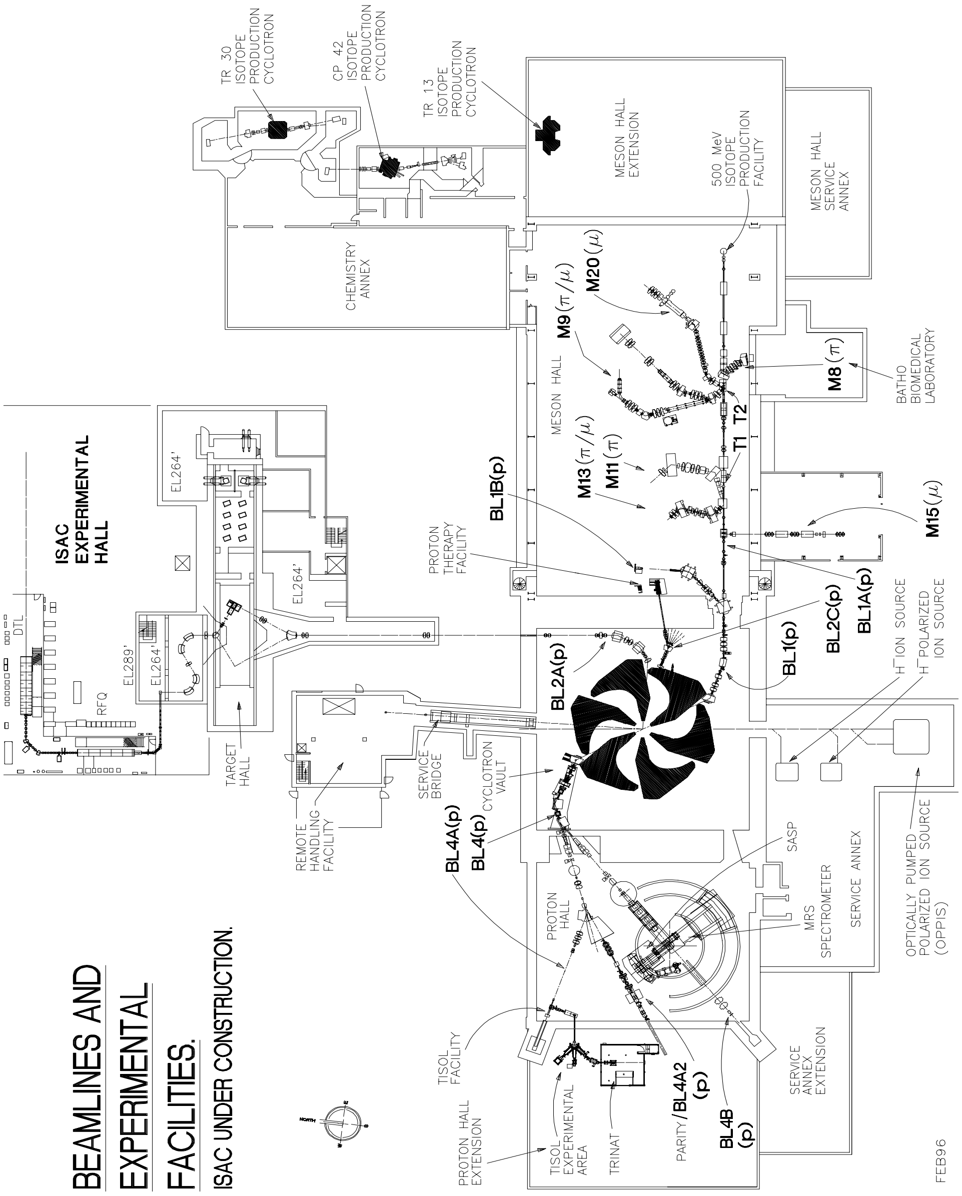

rest just within the surface of the pion production target decay to muons that need penetrate only a short distance (a fraction of a millimeter at most) to escape from the target into the beamline vacuum, with momenta up to the maximum of $p_{max} = 29.79$ MeV$/c$. The distribution of the muons from the pion decay is isotropic.

These muons have a range of about of 0.8 mm in graphite so they conveniently penetrate several thin windows but still stop in small samples, while the spin of the muons remains almost completely polarized. Surface muon beams are not mono-energetic since muons will come from pions decaying at various depths in the pion production target; those that start out deeper will lose more energy on their way out. The resulting muon flux rises with momentum, then drops sharply at the "surface muon edge" at p_{max}. The secondary beamline, with magnetic steering elements and positron separators (velocity selectors which remove positron contamination from the muon beam) are tuned to transport muons in a narrow momentum range $\triangle P/P$ of a few percent, with P chosen to be $\sim$1/2% below the surface muon edge, in order to achieve the greatest beam intensity.

The M11 beam line has two 60^{o} left bends and is 11 m long. Figure 3.2 shows the layout of the beam line and the location of the two foci and the slits. M11 may be considered to be composed of the following three sections:

- The front-end which separates the secondary pion beam from the primary proton beam.
- The middle section which defines the beam momentum, produces a dispersed double-focus at the mid-plane.
- The rear section which produces a doubly achromatic beam spot at the experimental target position.

Figure 3.2: Layout of M11 channel. The angle particles are emitted into M11 from the target relative to the incident proton beam is shown larger for clarity, in reality it is $\approx 3^{o}$.

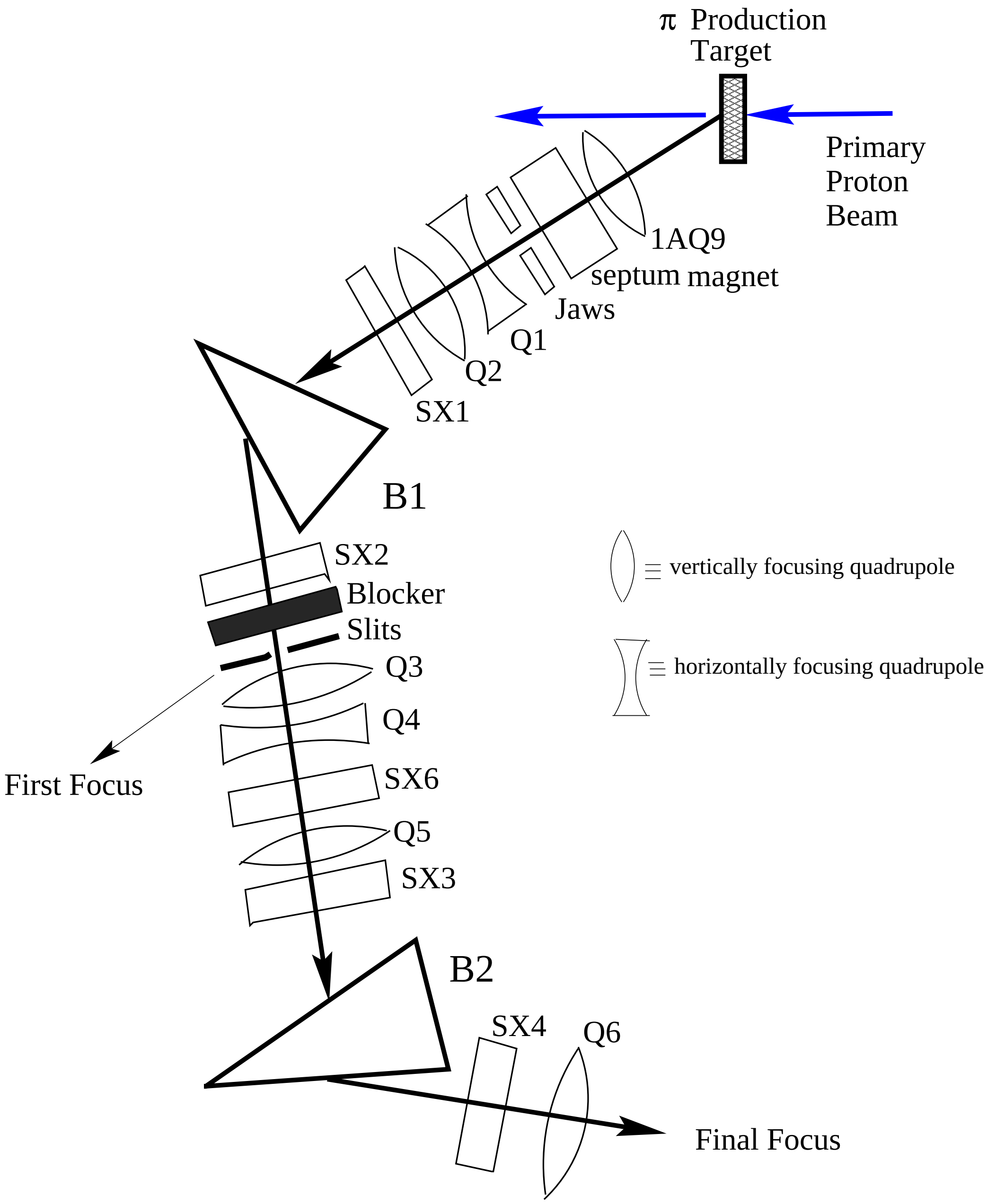

M11 has slits for selecting the desired particles at the momentum dispersed focus and the beam momentum acceptance. The momentum dispersion at the mid-plane is 18 mm per % $\frac{\triangle P}{P}$. One may choose the momentum bite by setting this midplane slit accordingly. In the experiment $\triangle$ P/P is chosen to be $\frac{1}{2}$%, i.e. M11 is tuned to transport muons in a momentum range $\triangle$P/P of $\frac{1}{2}$%.

The momentum of M11 is chosen by altering the current in the first dipole bending magnet via computer control to select various percentages of the initial reference momentum. The current in the other components in the beamline are set by tuning to optimize flux. From reference [9] the momentum of the pion beam in M11 is given by

$$P = [\{(\text{ B1 Magnetic field in gauss }) \times 0.03255\} - 0.26] \pm 0.25\% \text{ MeV}/c\ , \tag{3.1}$$

with no absorber in the mid-plane. No correction for absorber energy loss is needed since no absorber is included. However this calibration is low by 2%.

The maximum momentum available on M11 is 416 MeV/c limited by the septum magnet power supply. There is no minimum energy, although below 130 MeV/c it may be better to use M13 because of its larger solid angular acceptance [9].

Most runs were taken with a 100 μA proton beam.

3.2 Detector Set-up

Figure 3.3 illustrates the basic experimental arrangement. Muons were detected at the end of the secondary beam channel and in front of the stopping aluminum target with external and internal 0.25 mm thick plastic scintillator counters, C_{in} and C_{out} respectively. Range of 4.1 MeV muons in the counters is $\sim$ 1.3 mm.

The positron detector array consists of six scintillation counters, 6.4 mm thick, labelled:

1. F_{in} (inner forward),
2. B_{in} (inner backward),
3. F_{out} (outer forward),
4. B_{out} (outer backward),
5. U (upward), and
6. D (downward)

according to a "beam's eye view" naming convention.

The external magnetic field, provided by Helmholtz coils, is 70 gauss and is applied perpendicular to the muon polarization, causing the muon spins to undergo Larmor precession about the field. Since the decay e^+ will follow a helical path in the external field the dimensions of the positron detector array is such as to optimize its efficiency. For instance, at $p_e = 30$ MeV/c the radius of curvature ρ_e of an orbit perpendicular to $B = 70$ gauss (0.007 tesla) is 14.3 m , as given by the formula

$$\rho\ [\mathrm{m}] = \frac{p\ [\mathrm{MeV}/c]}{300 \times B\ [\mathrm{tesla}]}.$$

3.3 Stopping of the Polarized Muons in Aluminum

The muon stopping material is an aluminum sample of purity 99.999% and thickness 1.0 mm, contained in an evacuated cryostat at room temperature. With the

Figure 3.3: Side view of the detector setup

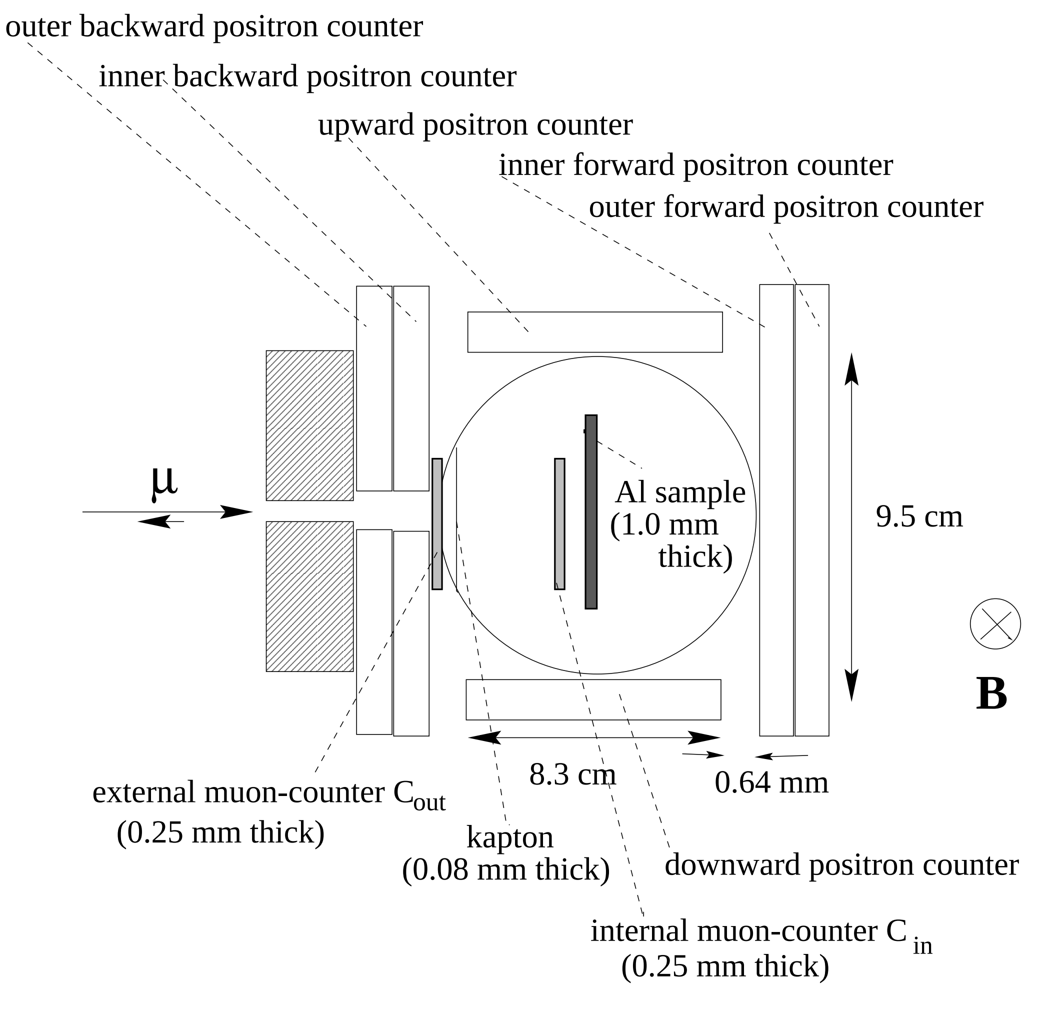

beamline tuned to 29.79 MeV/c selection is made for the muons coming only from the decay of pions that are at rest near the surface of the production target. This is because muons produced within the target lose momentum in making their way to the surface. The range of these 'surface muons' is small - approximately 0.6 mm in aluminum. Therefore, thin windows in the beamline and the cryostat are required to allow the muons to reach their destination. All of the surface muons are stopped in a thin target.

Stopping the polarized muons involves their implantation and thermalization in a medium. The slowing down and stopping of the muons in metals is a complex process. The time scales for the various processes by which the μ^+'s lose their kinetic energy are short. The μ^+'s are decelerated within 100 picoseconds, which is too rapid to allow any significant loss of polarization [11]. Also the primary processes bring into play only electrostatic interactions or electron scattering which are *not* spin-dependent [10].So there is rarely any loss of polarization during thermalization, especially in metallic samples [10].

Any variation of the local field between different occupation sites in the stopping sample will result in the muons dephasing as they precess, with a corresponding gradual loss of polarization described by a relaxation function. These characteristic frequencies and relaxation functions constitute the spectroscopy of the system. For aluminum the relaxation is negligible.

Furthermore it is now known that μ^+ depolarization is intimately related to the formation of muonium through electron capture (Mu = μ^+e^-) [12]. Whatever excitations of the medium that the muon passage may produce are quickly dissipated and the electronic structure "heals" by the time the muon reaches thermal energies. Polarized muons "see" an isotropic environment in aluminum. In fact, pure aluminum gives rise to practically no depolarization of μ^+ in the temperature range 1-300 K [13].

3.4 Electronics

An anticoincidence between the external muon counter and the internal decay positron counter is used as trigger, i.e. $C_{out}.\overline{F_{in}}$. Pulse-height and timing information were measured with analogue to digital converters (ADC's) (LeCroy 2249A and 2249W) and TDC's (LeCroy 4208 and 2228A). The TDC (LeCroy 4208) used for the muon decay time has a time resolution of 1 ns and the other which is used for the time of flight of the beam particles has a time resolution of $\frac{1}{4}$ ns. Events were recorded on tapes at a rate of $\sim 10^3\ s^{-1}$. Data aquisition was done using the VDACS acquisition system [14].

Raw counter pulses are fed to fast discriminators which generate logic pulses if the raw pulse height is above a set threshold. The logic pulses are then processed by the electronic circuit shown schematically in Figure 3.4. An incident muon generates a pulse in the muon counters, C_{out} and C_{in} . A trigger in C_{out} but not in the inner positron counter sends a start pulse to a fast digitizer (high-frequency "clock") of the 4208 TDC. Later the muon decays in the aluminum sample, triggering a stop pulse in the positron counters, which stops the clock. The time interval is digitized and the corresponding bin in a time histogram is incremented.

The method used to acumulate μSR histograms requires that only one muon be present in the sample at a time. This imposes a limit on the rate at which muons would be implanted in the sample (and therefore on the rate at which data can be accumulated). The probability of getting two muons is

$$P = R\tau,$$

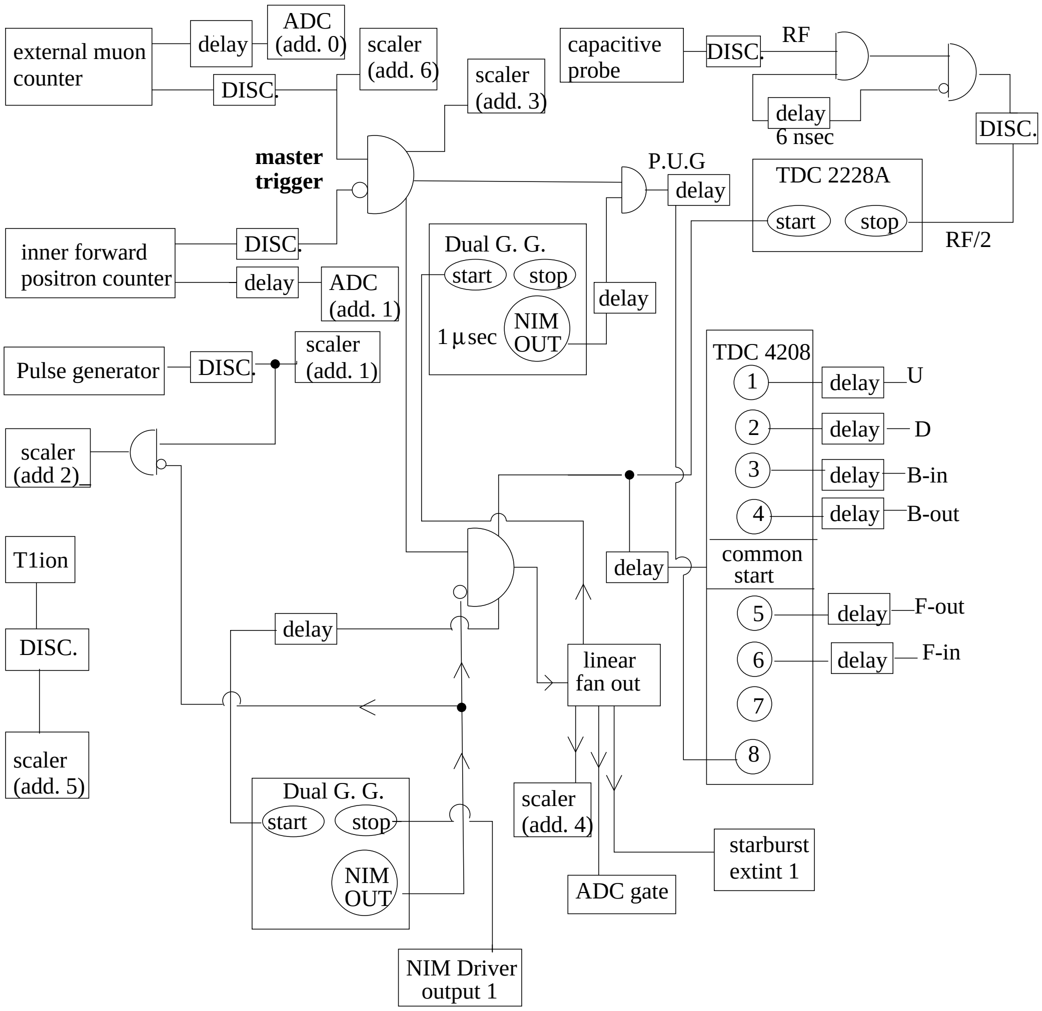

Figure 3.4: Electronics for data aquisition

where

$$R = \text{muon flux rate (Hz), and}$$

$$\tau = \text{“gate” time, i.e. maximum of } (t_{stop}\text{-}t_{start})$$

For $P \ll 1$, it is necessary to have $R \ll 1/\tau$. Muons are being delivered on M11 at a rate up to $\sim 10^3 s^{-1}$ and the time interval τ between a start pulse and a stop pulse is ≤ 9.7 microseconds. So the probability of a second muon entering the system while the decay time of the first muon is being measured is $\sim 1\%$. The histogram incremented by the pile-up-gate is for counting events with pile-up muons throughout the gate τ.

The TDC (LeCroy 2228A) is started by the event trigger and stopped by the cyclotron capacitive probe pulse prescaled by 1/2. The division by 2 gives a stop as much as twice the cyclotron period after the start. This allows a complete RF cycle to be observed without distortion from the edges of the coincidence overlap in the event trigger hardware.

Chapter 4

DATA ANALYSIS AND RESULTS

4.1 Choosing the momentum of M11

The beam test was done only for positive particles at several momenta in the range a few percent below and above 30 MeV/c. The reference tune used for the M11 beam line is shown in Table 4.1 below. Since the momentum calibration given by equation 3.1 is not quite right, the momenta were calculated by simple scaling based on the fact that this particular setting is found to be at a momentum 1/4 % below the $\mu - \pi$ edge, i.e. the reference momentum chosen is 29.72 MeV/c. The $\mu - \pi$ edge occurs at 29.79 MeV/c, the momentum at which a muon is produced from a pion decaying at rest. To pick a momentum at, e.g. 1% above the reference momentum of 29.72 MeV/c, the following procedures are taken:

- the beam line is adjusted via computer control through the command "m11 scale by 1 %"
- some time is allowed for the the current in the elements to stabilize to their new values

- the current in B2 is adjusted so that the ratio of the fluxes, B1 and B2 (from NMR read-outs) is 1.025
- the current in the septum magnet is adjusted so that the ratio of the flux in B1 (from NMR read-out) to the current in the septum = 3.012.

Reference Tune Chosen for M11		
Element	**DAC**	**Current (A)**
B1	34128	49.32
B2	28798	31.86
Q1	510	22.95
Q2	482	20.26
Q3	559	25.39
Q4	29802	44.68
Q5	480	22.71
Q6	878	42.97
SX1	113	13.96
SX2	222	2.25
SX3	957	7.62
SX4	599	5.96
SX2.5	204	2.15
Septum	2312	301.18
1AQ9	35154	40.28

Table 4.1: Setting of the M11 components at the reference momentum.

As the momentum of the beamline was changed in steps of 1/4% from the reference momentum chosen at 29.72 MeV/c it was found that the hysteresis level is 0.03 %, i.e. the magnetic field intensity, measured using an NMR probe, in the benders B1 and B2 (see Figure 3.2) is reproducible up to within 0.03%.

Data was analyzed on line and off line using the NOVA data analysis system [15]. Electrons, muons, and pions were distinguished when possible in the thin counters C_{in} and C_{out} by pulse height and by timing against the machine RF signal.

4.2 Transition at the $\mu - \pi$ edge

An interesting feature of the surface muons produced in the target is that they occur up to beamline momentum of 29.79 MeV/c, (the $\mu - \pi$ edge), whereas positrons, cloud muons and pions are transported at a wide range of momentum. Muon clouds originate from pion decays outside, but in the vicinity of the target with the right momentum and direction necessary to make it through the beam transport system.

Figure 4.1 shows the time of flight of the M11 beam relative to the cyclotron RF at $p = 29.8$ MeV/c, 30.4 MeV/c (2% above the $\mu - \pi$ edge) and 33.1 MeV/c (11% above the edge). The raw TOF spectra are obtained without any cut and the spectra with ADC cut are obtained by selecting events with ADC channel greater than 130 for the external C_{out} counter. This cut is made to partially suppress the e^+'s. Note that the horizontal axis runs backward in time since the 2228A TDC is started by the event trigger and stopped by the cyclotron RF. The following six properties are observed from Figure 4.1:

- The characteristic exponential decrease in the surface μ^+ flux with time due to pion at rest with a mean life of 26 ns, in Figure 4.1(b). Figure 4.1(b) is the time of flight spectrum at 29.8 MeV/c with partial positron suppression.

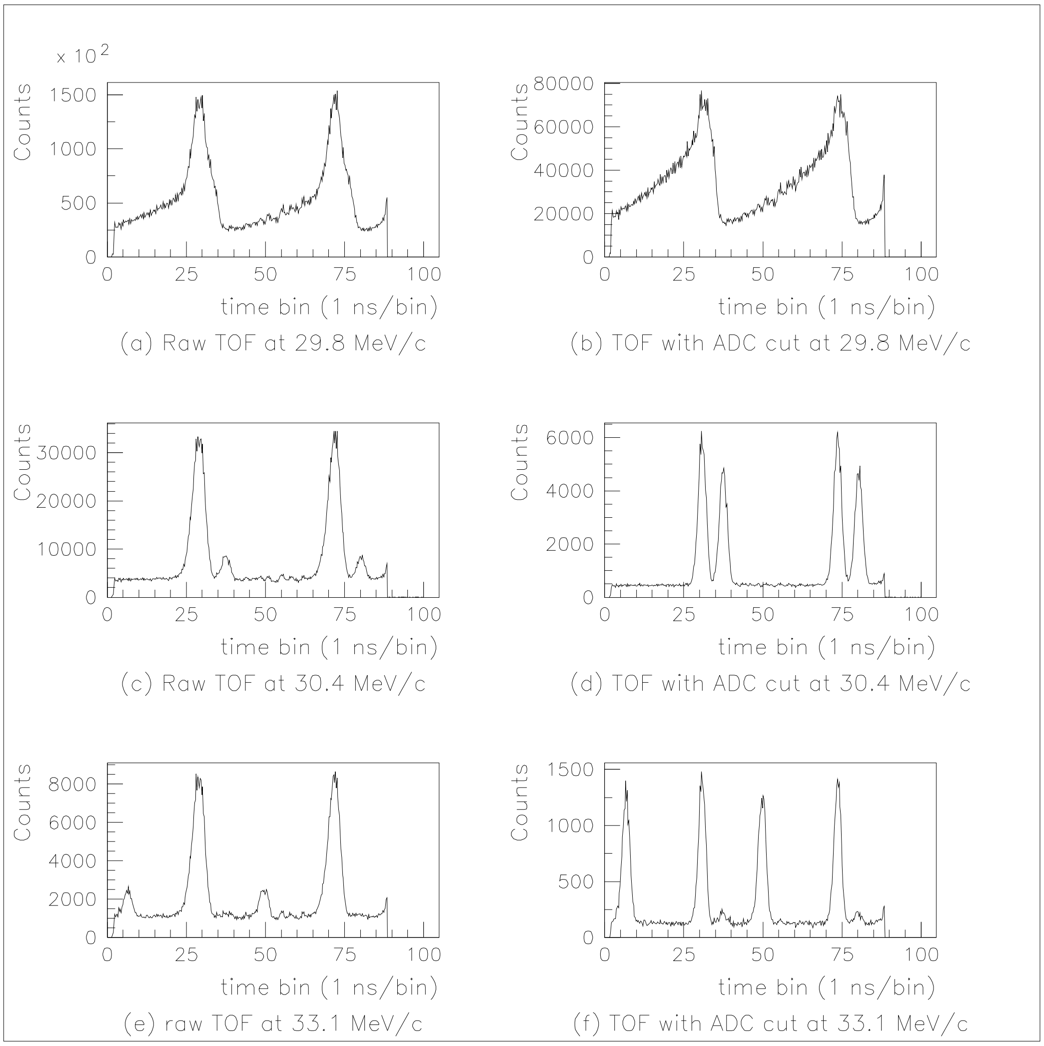

Figure 4.1: Transition at the $\mu - \pi$ edge. The ADC cut (ADC1 $>$ 130, see Figure 4.2) on the pulse height distribution for the C_{out} is to partially suppress the positrons in the time of flight spectra. The horizontal axis runs backward in time.

- The negligible existence of surface μ^+ at momenta above the $\mu - \pi$ edge as seen from the absence of the exponential decrease in flux with time.

- The cloud μ^+ which has the property of being time correlated becomes noticeable above the $\mu - \pi$ edge. The cloud μ^+ peak walks across the TOF spectrum with change in momentum. The difference in flight time for μ^+ relative to e^+ is determined by the length of the flight path and the particle masses.

- The flat background of e^+'s from $\mu^+ \rightarrow e^+\nu\bar{\nu}$ decay following $\pi^+ \rightarrow \mu^+\nu$ decay.

- The e^+ peak which are time correlated with the cyclotron RF signal from $\pi^0 \rightarrow \gamma\gamma$ decays in the production target whereby a photon is converted to an $\mathrm{e^+e^-}$ pair [16, 17].

- The π^+ peak becomes noticeable above the $\mu - \pi$ edge in Figure 4.1(f), the time of flight with partial positron suppression at 33.1 MeV/c.

4.3 Event selection (background positrons)

The raw pulse height distribution in C_{in} and C_{out} (Figure 4.2) at 29.79 MeV/c shows that the amount of positrons is not negligible but not overwhelming. In fact, as will be seen later, the ratio of positron to muon is ~1:1. The positrons appear to have a higher energy loss in the C_{out} counter than in the C_{in} counter. There is a definite pulse shape difference between muons and positrons in the pulse height distribution in C_{in} and C_{out} (Figure 4.2). It is not possible to have a cut in the energy loss in C_{out} which would be good enough to suppress the positrons with negligible loss in muons (μ^+'s). To suppress the positron background to a trivial level, the off-line selection on ADC channel higher than

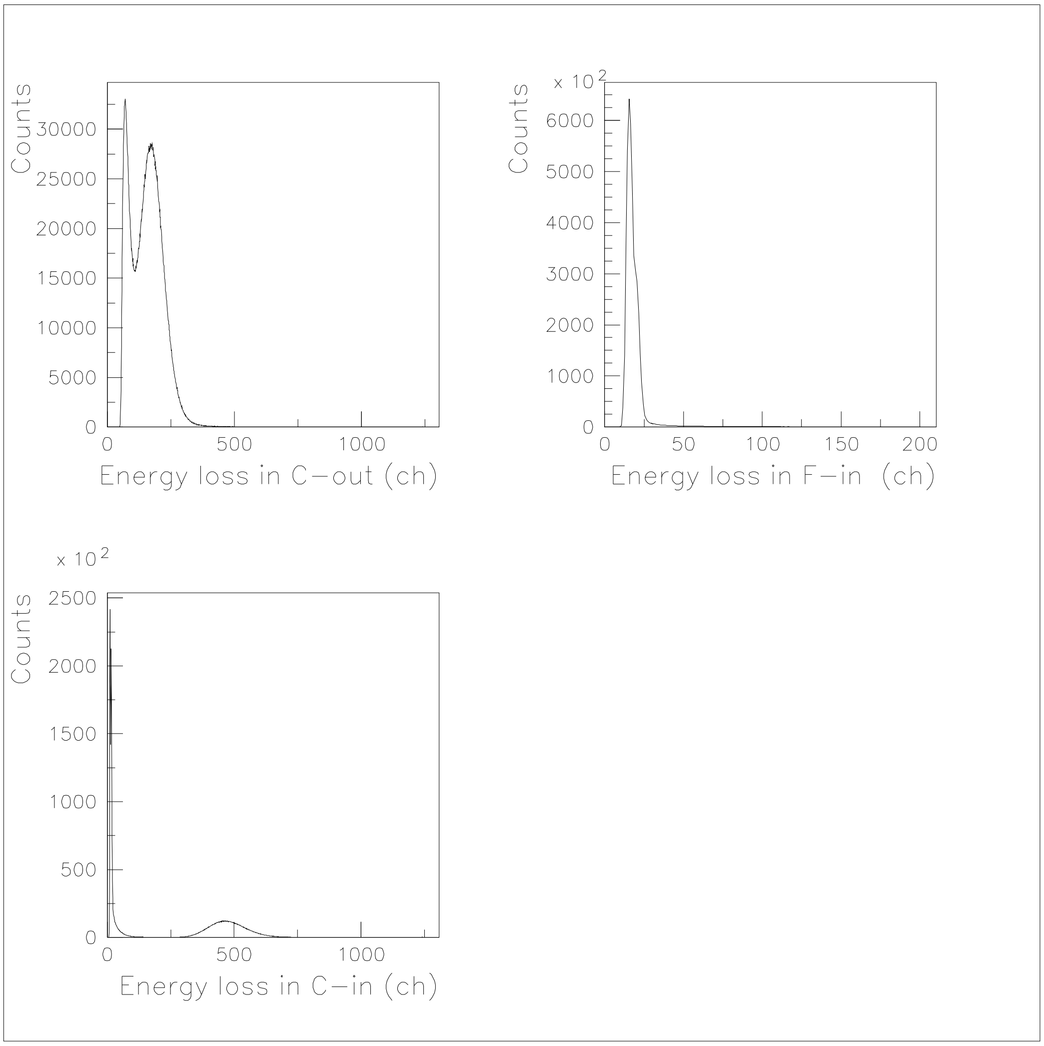

Figure 4.2: Pulse height spectra without cuts at a momentum when the surface μ^+ flux is high at the $\mu - \pi$ edge.

200 for the C_{in} counter was applied. The cut reduced the positron background to ~1% of the total μ^+ flux, without any cut applied to the C_{out} counter.

4.4 Particle Fluxes

The fluxes for (surface and cloud) muons and the positrons are plotted in Figure 4.3. The slits are 9 mm open giving a $\triangle$P/P of $\frac{1}{2}$% (the channel transmission reaches its maximum at $\sim$ 100 mm with $\triangle$P/P = 5%). Only the pulse height distribution of the C_{in} counter was used to calculate the flux because of the clean cut available on it to separate the μ^+'s from the e^+'s. The flux at other momenta using this method is not available because of lack of data. The variation in e^+ flux with momentum follows the same trend as that of the μ^+'s which indicates that a large portion of the e^+'s comes from muon decay in the detector setup. It must be noted that there are many positrons that could pass uncounted because they are below the threshold of the C_{in} counter.

The appearance of pions (π^+'s) is seen from the time of flight spectrum (see Figure 4.1(f)) only at 33.1 MeV/c which is the highest momentum M11 was run at in the beam test. On applying cuts, summing over the π^+ peak and making correction for the flat background positrons in the TOF spectrum , the π^+ flux is 0.018 ± 0.001 counts/(μA sec) which is $\approx$ 7 % of the cloud μ^+ flux. Note that 33.1 MeV/c muons (with a kinetic energy of 5.1 MeV) have a range of 1.0 mm in aluminum. Thus muons beyond that momentum will pass uncounted because they will go through the 1.0 mm thick aluminum target and then vetoed in the trigger by hitting the F_{in} counter.

Particle fluxes with computer live time corrections were calculated as follows:

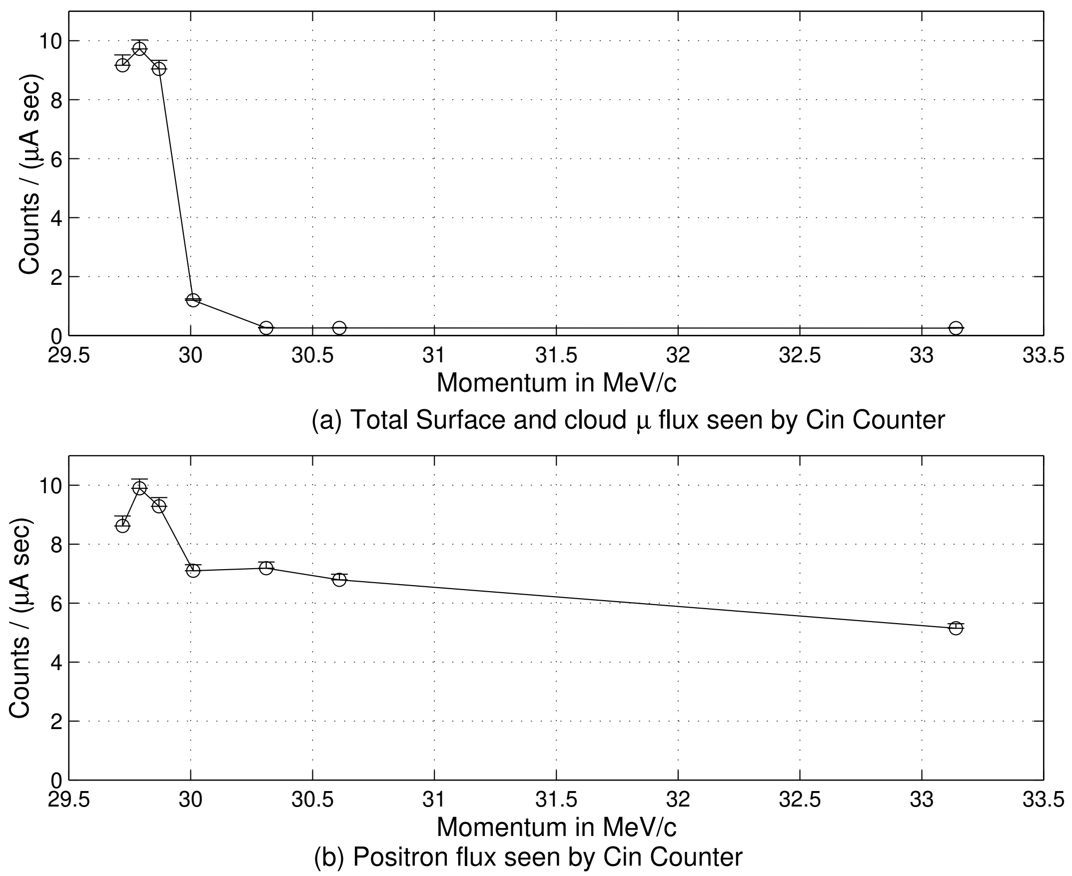

Figure 4.3: Change in flux of (cloud and surface) μ^+ and e^+ with momentum at $\triangle P/P = \frac{1}{2}\%$. The μ^+ flux is highest at the $\mu - \pi$ edge ($p = 29.79$ MeV$/c$). Note that there are many positrons that could pass "unseen" by the C_{in} counter.

$$\mu \text{ flux in counts per } (\mu\text{A second})$$

$$= \frac{\text{sum of counts in the } \mu \text{ peak of the } C_{in} \text{ pulse height spectrum}}{\text{total T1-ion counts}}$$

$$\times \frac{\text{T1-ion count rate per } \mu\text{A current of the primary proton beam}}{\text{computer live time fraction}}.$$

The total T1-ion count rate per μA current of the primary proton beam is obtained by calculating the average

$$\left\langle \frac{\text{T1-ion flux rate from the visual scalers}}{\text{instantaneous proton beam current}} \right\rangle = 267.4 \pm 7.0 \text{counts}/(\mu\text{A sec}).$$

The primary proton beam current was usually not constant and varied from 98 μA to 133 μA and was sometimes off for a while during which the analysis is stopped. The computer live time fraction is given by:

$$\text{live time fraction} = \frac{\text{total triggers when the computer is not busy}}{\text{total triggers}},$$

where the trigger is the anticoincidence $C_{out}.\overline{F_{in}}$. The live time fraction varied from 56 % to 86 % at momenta when the surface muon flux is high and zero respectively.

4.5 Fit For The Determination Of The Asymmetry

The transverse-field muon-precession data are normally analyzed with the expression

$$N(\mathrm{t}) = N_o \exp(-\mathrm{t}/\mathrm{t}_\mu)[1 + \alpha P(t) \cos \omega \mathrm{t} + \phi] + Bkg, \tag{4.1}$$

where t_μ=2.20 μs is the mean lifetime of the muon, ω is the precession frequency, α is the the muon decay asymmetry, and *Bkg* is the accidental flat background. Relaxation of the polarization *P(t)* is typically taken as either Gaussian $\exp(-\sigma^2 t^2)$ or exponential $\exp(-\lambda t)$ [13]. The impurities in the aluminum sample are low enough to neglect the effect of depolarization of the μ^+ as it is implanted and stopped in the sample (i.e., $P(t) = 1$, in the analysis). The free parameters are N_o, α, ω, ϕ and *Bkg*. These are referred to as P_1, P_2, P_3, P_4, and P_5 by the fitting software.

Each of the six positron counters in Figure 3.3 behaves as a single detector. However only the upward and downward counters are used to determine the asymmetry and polarization because the data has a smaller background. Figure 4.4 shows the time spectrum of the six counters without cuts; the positron background contamination is worse in forward-decay beams.

Figure 4.5 shows the variation in the asymmetry of the raw signal (with no cuts applied) from the upward and downward e^+ counters with momentum in the range ~2% above and below the $\mu - \pi$ edge (29.8 MeV/c). The data includes background e^+'s and cloud μ^+'s. It is expected that the asymmetry of the surface muons is nearest to 1/3 at 29.8 MeV/c, see Table 4.2. From Table 4.2, it is seen that there is an uncertainty of 1/4% in the value of the momentum at the $\mu - \pi$ edge. The pulse height distribution in C_{in} is not available to suppress the background e^+'s at all the momenta in Figure 4.5, since the threshold level of the discriminator from the C_{in} counter was too high. From here onwards, only the downward positron counter is used to analyze the beam polarization.

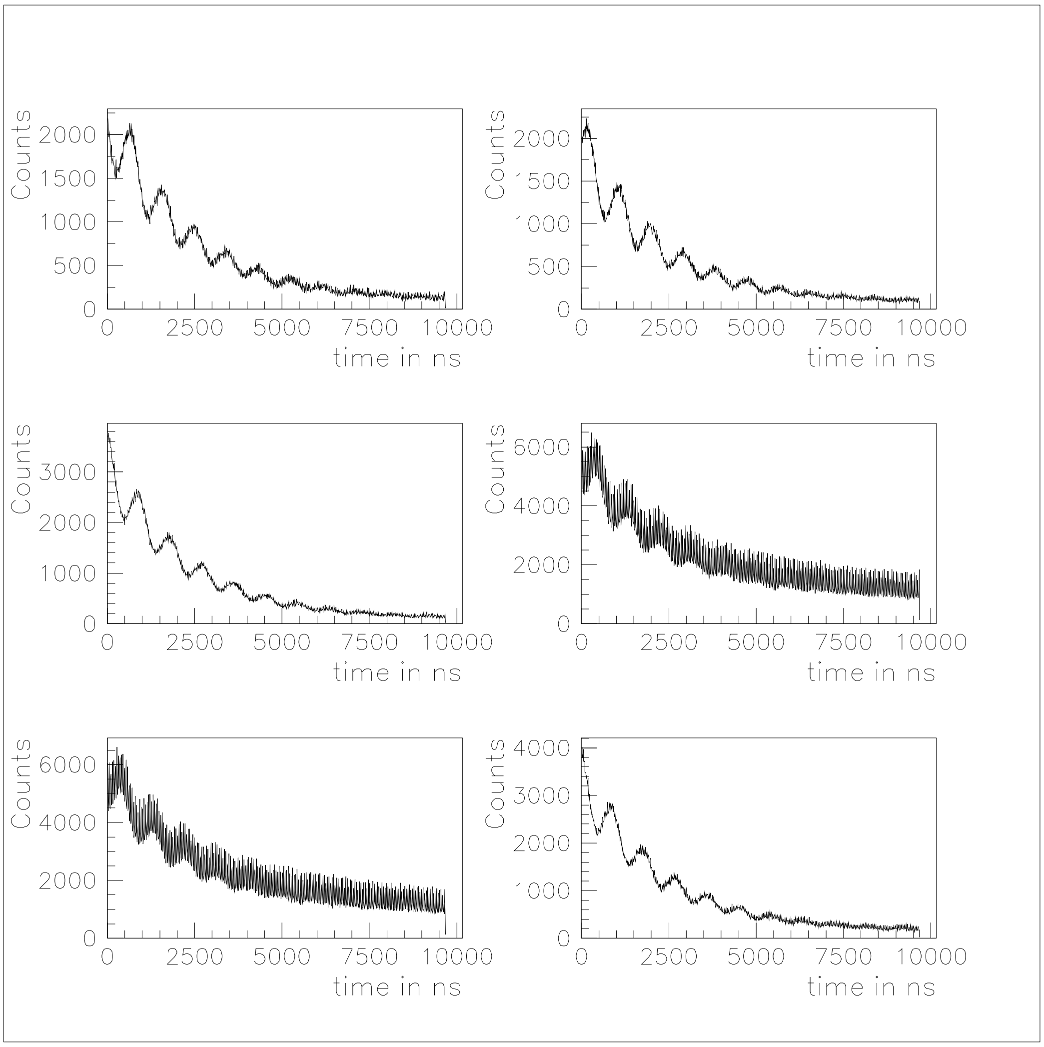

Figure 4.4: Time spectra of the positron counters U, D, B_{in}, F_{in}, F_{out}, B_{out} without cuts (row by row from left to right).

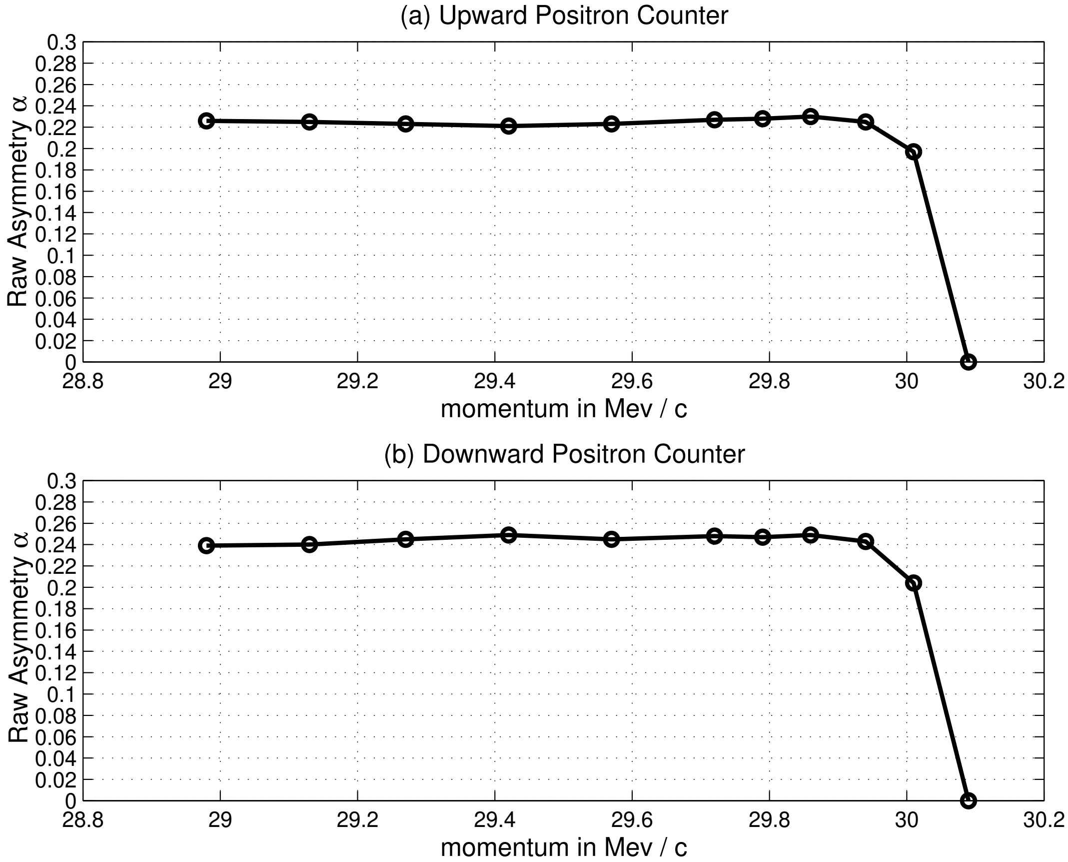

Figure 4.5: Raw asymmetry, α, of signal from (a) the upward e^+ counter and (b) downward positron counter. Statistical error in α is negligible and the background includes cloud μ^+'s, beam e^+'s and e^+'s from μ^+ decay in the detector setup.

Momentum	**upward e^+ counter**		**downward e^+ counter**	
in MeV/c	**raw α**	**α with ADC cut**	**raw α**	**α with ADC cut**
29.72	0.227	0.265	0.248	0.277
29.79	0.228	0.268	0.247	0.275
29.87	0.230	0.263	0.249	0.279
30.01	0.197	0.222	0.205	0.227

Table 4.2: Asymmetry of the surface muons at different momenta about the $\mu-\pi$ edge from the upward and downward positron counters. The statistical error is negligible.

4.6 Pile-up gate

The logic for the pile-up gate trigger is

$$\text{P.U.G.} = \text{trigger.(delayed trigger.}\overline{BUSY}\text{)}.$$

Here, only the case at $p = 29.79$ MeV/c is considered. The flat pile-up time spectrum in Figure 4.6(a), apart from the sharp peak shows that pile-up particles are arriving at random in time in the time gate. Pile-up muons are the muons arriving in the "μSR" time gate τ of ~ 9.7 μs followed by another particle. The latter can be a positron, a pion or another muon. If the second particle is a muon, the determination of the decay time will be uncertain, invalidating the determination of the decay asymmetry. On summing for the pile-up muons in the pulse height distribution for pile-up particles in the C_{in} scintillation counter (see Figure 4.6(e)) , their contribution is 2.7% of the total μ^+ flux. This value agrees with the estimation made in section 3.4. The pile-up muons in the sharp peak amount to 0.26 % of the total μ^+ flux.

The time of flight distributions for the pile-up gate in Figures 4.6(c) and (d) show that the pile-up particles are surface muons and positrons. The pile-up

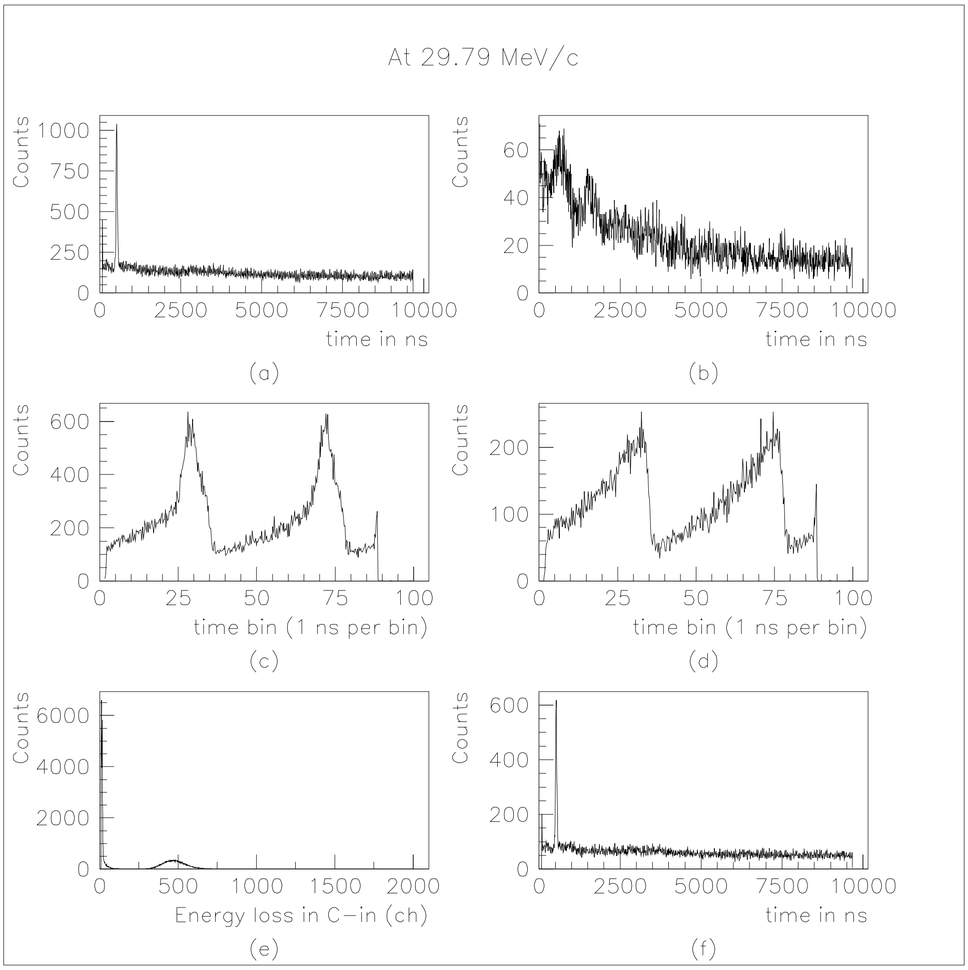

Figure 4.6: (a) Pile-up gate time spectrum with no cuts, (b) time spectrum for pile-up particles in upward e^+-counter, (c) TOF of pile-up particles, (d) TOF of pile-up particles with positron suppression , (e) pulse height distribution for pile-up particles in the C_{in} scintillation counter, (e) Pile-up gate time spectrum with positron suppression.

particles going in the U counter have a polarization of 75.5 $\pm$ 0.9 % (see the asymmetry fit in Figure 4.7). On the other hand polarization of the pile-up muons arriving after the sharp peak in the positron counter U in the time gate has a polarization of 99.9 $\pm$ 1.5 % .

There was no provision in the electronics to reject these pile-up muons. The rejection was done in the analysis. It will be seen in the last section of this chapter that the distortion in the μSR spectra due to the pile-up particles is negligible. Hence the probability that a second surface muon enters the time gate τ is negligible. The pile-up gate more likely is set by a positron following a muon into the system. This would imply that the positron flux is a few times greater than the muon flux.

4.7 Cloud μ^+, its flux and polarization

Whether the cloud μ^+'s at the selected momenta are polarized or have a polarization opposite to that of surface μ^+'s is questionable. Four runs above the $\mu-\pi$ edge, where there are no apparent surface μ^+'s, are chosen to deal with this issue. Time of flight cuts were applied to the latter to select cloud μ^+'s. Also pulse height cuts are applied to suppress the flat background of decay positrons.

There is no convergence when the fitting Equation 4.1 is applied to the cloud muon data sample. Figure 4.8 shows the time spectra for positron decay from cloud muons at 30.1, 30.5, 30.6 and 33.1 MeV/c. They are fitted with the exponential fit

$$N(\mathrm{t}) = N_o \exp(\mathrm{t}/\mathrm{t}_\mu) + Bkg, \tag{4.2}$$

where $\mathrm{t}_\mu = 2.20$ μs is the mean lifetime of the muon, and Bkg is the accidental flat background. The free parameters are N_o, t_μ and Bkg referred to as P_1, P_2

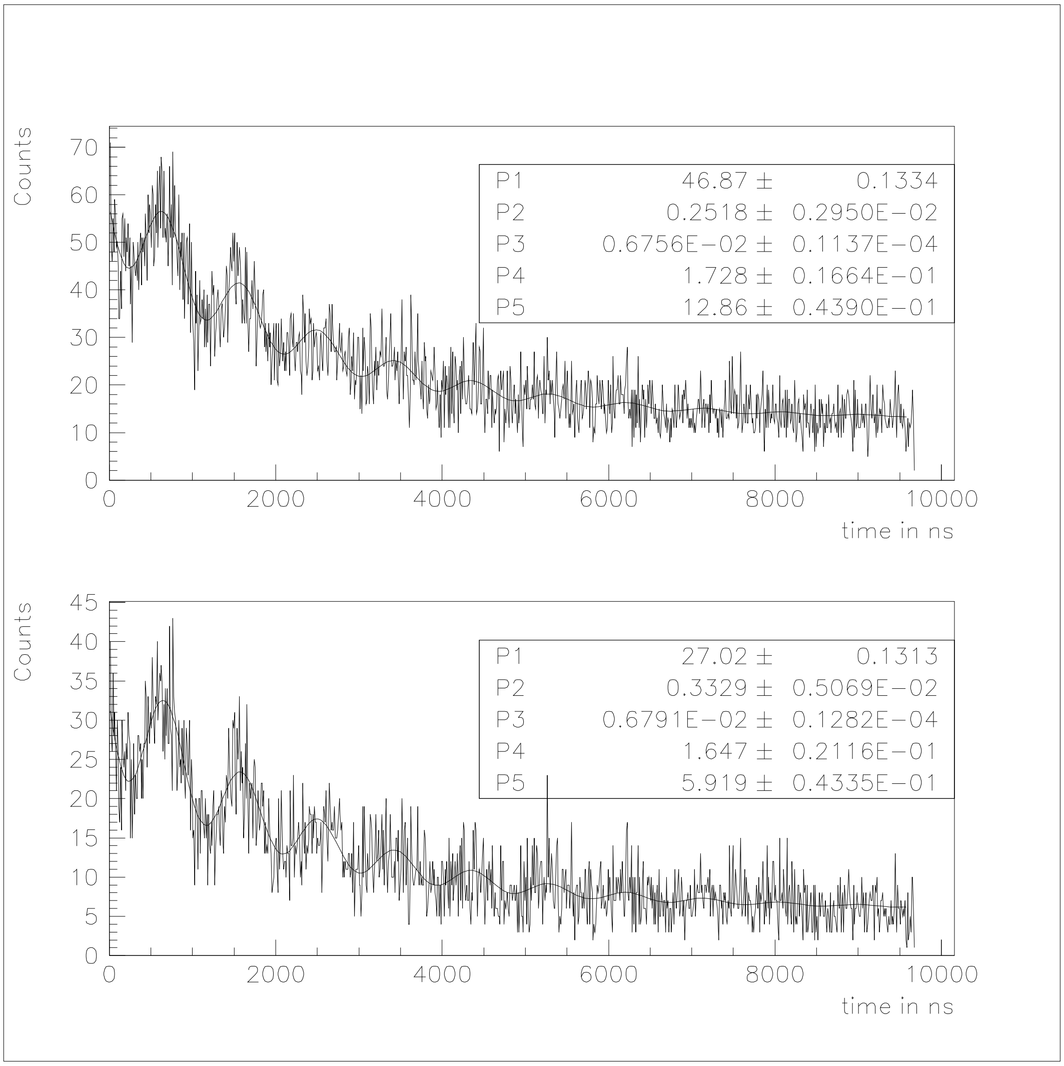

Figure 4.7: Above: the asymmetry for the decay of the pile-up muons, with no cuts, in counter U is 0.252 ± 0.003. Below: the fit for asymmetry for the decay of the pile-up muons, with positron suppression, arriving in counter U after the sharp peak in the time gate (see Figure 4.6(a)); it is 0.333 ± 0.005.

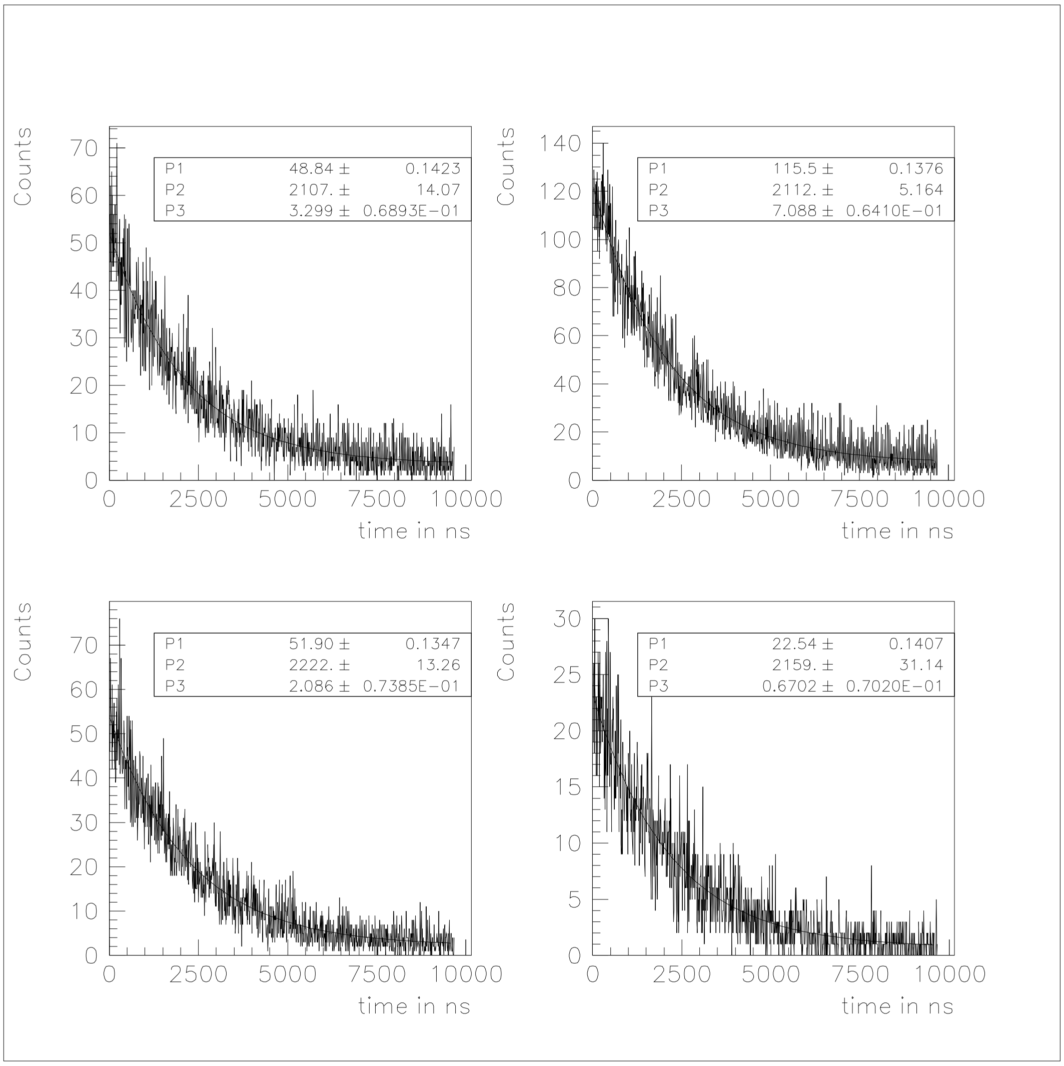

Figure 4.8: Spectra of e^+ decay from cloud μ^+'s at 30.1, 30.5, 30.6 and 33.1 MeV/c; the absence of sinusoidal variation verifies the fact that the cloud μ^+'s are not polarized.

and P_3 by the fitting software. The absence of sinusoidal variation verifies the fact that the cloud μ^+'s are not polarized. The fitting value for t_μ is best for the bottom left spectrum at 30.6 MeV/c because for this particular run there is more data and the pulse height distribution for the C_{in} counter is available for a better suppression of background decay positrons.

The highest momentum at which the beamline M11 was run is 33.1 MeV/c. From 30.3 to 33.1 MeV/c, where there is cloud μ^+ and no apparent surface μ^+, the total μ^+ flux, is calculated using the method in the section on "Particle Fluxes". It is almost constant at 0.25 ± 0.02 counts/(μA second) (see Figure 4.3). It is extrapolated that at the $\mu - \pi$ edge, at 29.8 MeV/c, the cloud μ^+ flux has the same value.

The following is an argument to explain why the cloud muon does not have a polarization opposite to that of the surface muon. When the beamline is tuned for a momentum above the $\mu - \pi$ edge that momentum can be the sum of momenta of a pion with a few MeV/c directed into the beamline and a muon decaying in the same direction, as exemplified in Figure 4.9(a). There is also the case where the pion has a momentum larger than the beamline tune momentum and the muon decaying in the backward direction, as illustrated in Figure 4.9(b). The muon in the the first case will have a polarization opposite of that in the second case. The absence of the sinusoidal variation in the spectra in Figure 4.8, implying zero polarization, shows that the two possibilities occur with equal probability at the angle of 2.5^o at which M11 views the π production target. Cloud muons decrease the apparent polarization of the surface beam by the same percentage of cloud muons in the beamline .

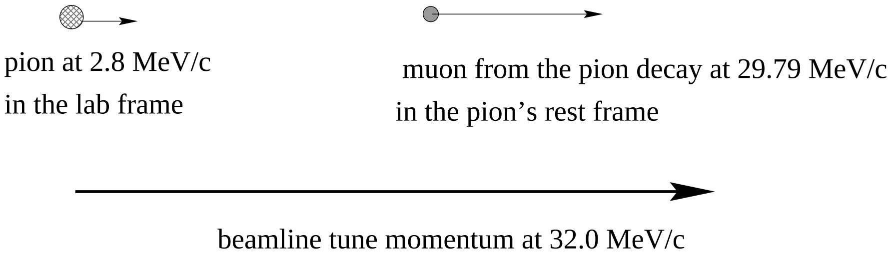

(a) The muon coming off in the forward direction.

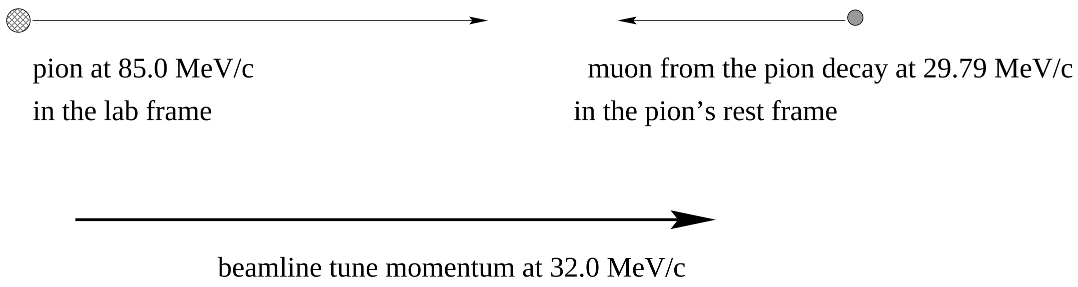

(b) The muon coming off in the backward direction.

Figure 4.9: Momentum of muon from pion decay in flight above the $\mu - \pi$ edge, at a beamline tune momentum $p = 32.0$ MeVc.

4.8 Some features across the RF cycle at the $\mu - \pi$ edge

At the $\mu - \pi$ edge ($p = 29.79$ MeV/c), the flux of surface muons is at a maximum. In order to obtain a surface muon flux with minimum background contamination and hence optimizing the beam polarization, a detailed analysis of some important features is done across the RF cyclotron period. The latter is of a duration of 43.5 nanoseconds; it is divided into six bins of 7.25 nanoseconds. The RF period is chosen between two maxima in the surface muon flux in the TOF spectrum in Figure 4.14(a). Figure 4.14(a) shows the time of flight spectrum at the $\mu - \pi$ edge with pulse height cut for positron suppression. The TOF spectrum is for one RF cycle from 32.5 ns to 76.0 ns. The flux of the different particles and the asymmetry of the muon decay are investigated in these bins and a time window in the TOF spectrum is then selected in which there are essentially no contaminant particles.

4.8.1 μ^+, e^+ and π^+, Their Flux and Time of Arrival

Figure 4.10 shows the variation in total (surface and cloud) muon flux and the positron flux at the $\mu - \pi$ edge ($p = 29.79$ MeV/c). By referring to Figure 4.1 it can be deduced that the beam positrons arrive in the 1st and 6th bins.

Based on the fact that the beam e^+ peak does not move with a change in momentum of the beam; because due to small positron mass it travels with a velocity very close to the speed of light from the 1AT1 production target; and from the TOF spectra at 29.9 MeV/c, 30.0 MeV/c and 30.1 MeV/c in Figure 4.11, the following observations are made (a more detailed analysis is made in the following sections):

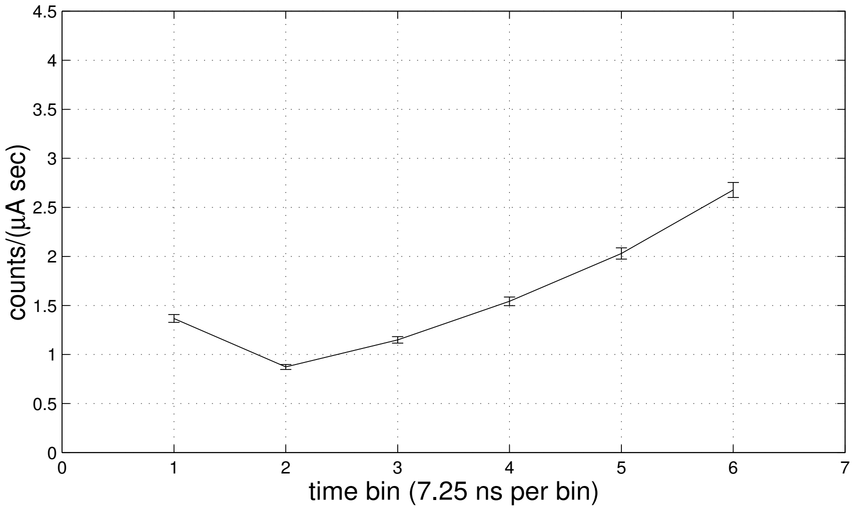

(a) Total Surface and cloud muon flux

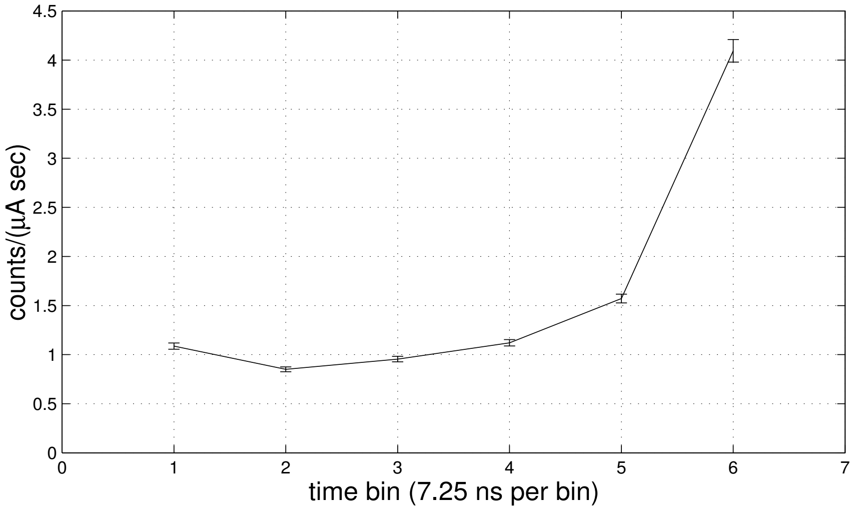

(b) Positron flux

Figure 4.10: (a) Total muon flux and, (b) total positron flux, across one RF cycle divided into six bins at the $\mu - \pi$ edge. The horizontal axis goes backward in time.

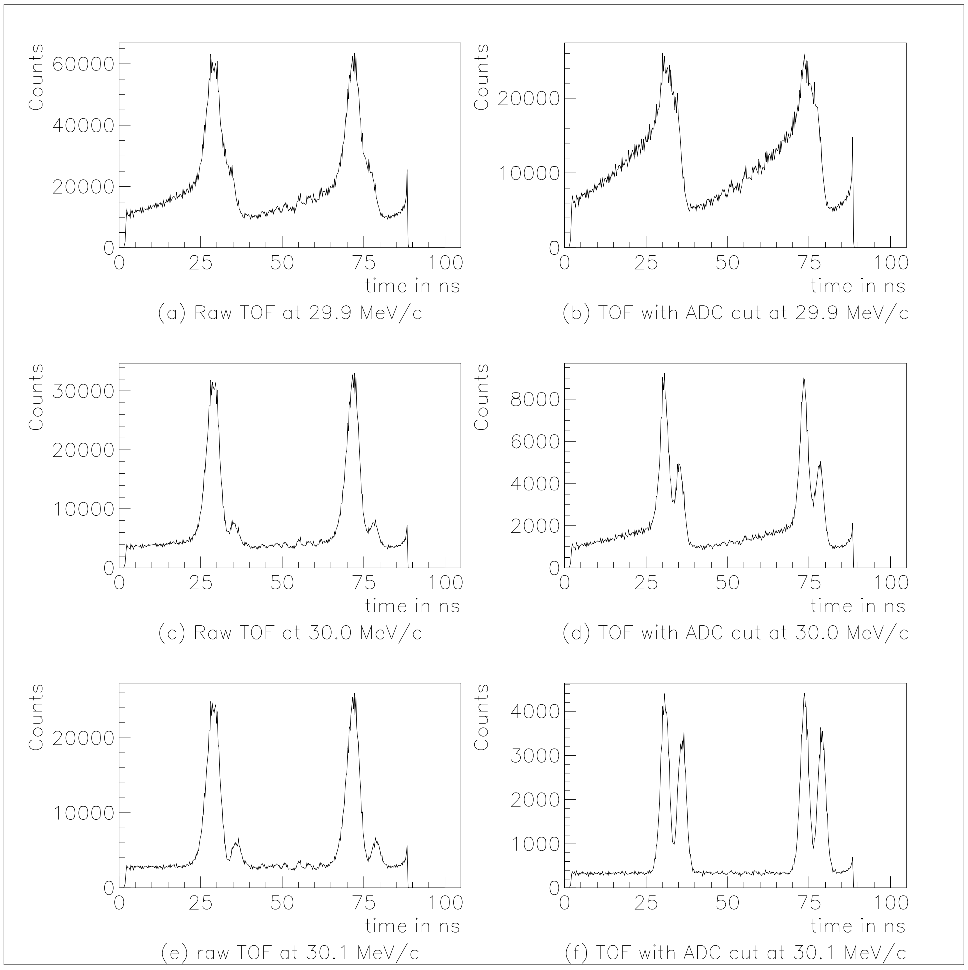

Figure 4.11: From these TOF spectra it is concluded that the beam e^+ and the cloud μ^+ peaks arrive almost in time at the $\mu - \pi$ edge at 29.8 MeV/c. Note: the horizontal axis goes backward in time.

- At the $\mu - \pi$ edge (29.8 MeV/c), the cloud muon peak arrives almost in time with the beam e^+'s which are time correlated with the cyclotron RF.
- At 29.8 MeV/c both the beam e^+'s and the cloud μ^+ peaks arrive almost in time with the sharp rise in surface μ^+ flux in the TOF spectrum.

Hence, unwanted beam positrons and cloud muons appear in the first and sixth bins.

Pions are time correlated to the RF cycle since they originate from the production target. Because the pion is more massive than muon or positron, the pion peak is expected to arrive later than the beam positron and cloud muon peaks (see Table 4.3 below). Thus, at the $\mu - \pi$ edge, pions arriving at a negligibly small rate of ~0.02 counts/(μA second) are also overlapping with the cloud muon and beam positrons peaks too.

Particle	**mass in MeV/c^2**	**mean life**	**flight time**
e^+	0.51099907(15)	stable	37 ns
μ^+	105.658389(34)	2.19703(4) μs	135 ns
π^+	139.56995(35)	26.033(5) ns	176 ns

Table 4.3: Particle mass, mean life and flight time. The flight time is for 29.8 MeV/c, the nominal length of M11 channel is 11 m and the cyclotron period is 43.6 ns.

4.8.2 Cloud Muon Movement in TOF Spectrum

The movement of the cloud muon peak from p = 30.3 MeV/c in Figure 4.12(b) to p = 29.8 MeV/c in Figure 4.12(a) can be calculated kinematically. The velocity(v) and momentum (p) of a muon are related by

$$p_\mu = \gamma_\mu m_\mu v_\mu,$$

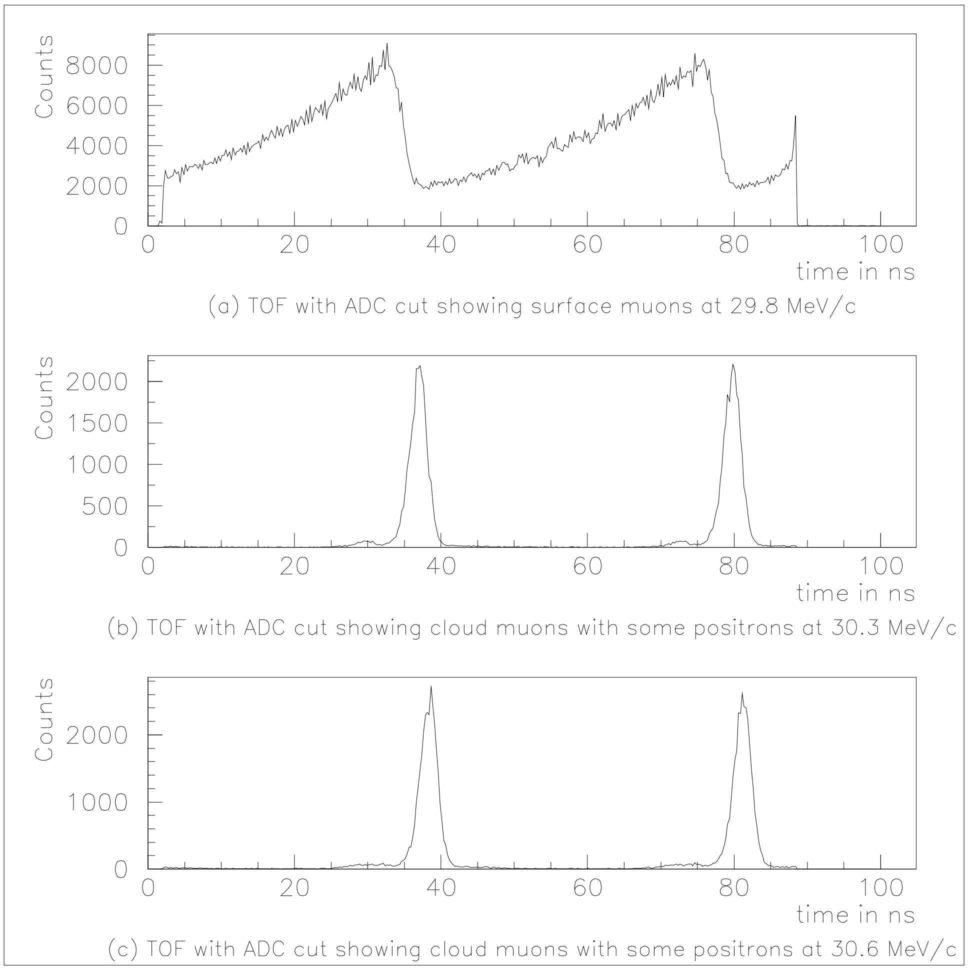

Figure 4.12: At 29.8 MeV/c, the cloud muon peaks arrive in the TOF spectrum earlier than at 30.3 MeV/c, they will sit about the sharp fall in the surface μ^+ flux near to the unsuppressed beam e^+. Note: the horizontal axis goes backward in time.

where m_μ is the rest mass of the muon and γ_μ is the relativistic factor given by

$$\gamma_\mu = \frac{1}{\sqrt{1-\left(\frac{v_\mu}{c}\right)^2}}.$$

The above equations can be rearranged to give

$$\frac{v_\mu}{c} = \sqrt{\frac{{p_\mu}^2}{{p_\mu}^2 + {m_\mu}^2}}.$$

Assuming that the cloud muons originate near the 1AT1 pion production target, the time of flight of the muons through the M11 channel is

$$t_\mu = \frac{d}{v_\mu},$$

where $d = 11$ m is the length of the M11 channel in the lab frame. For a small change $\triangle p/p$ = -1.7 % from p = 30.3 MeV/c to p = 29.8 MeV/c, $\triangle t_\mu$ = 2.0 nanoseconds. The formula used is

$$\triangle t_\mu = -\frac{d}{c}\frac{{m_\mu}^2}{{p_\mu}^2}\sqrt{\frac{{p_\mu}^2}{{p_\mu}^2 + {m_\mu}^2}}\frac{\triangle p_\mu}{p_\mu}.$$

The calculation is verified for the movement of the muon clouds in the TOF when p changes from 30.3 MeV/c (Figure 4.12(b)) to 30.6 MeV/c (Figure 4.12(c)); the calculated $\triangle t_\mu = 1.2$ nanoseconds whereas the measured $\triangle t_\mu = 1.4$ nanoseconds. There is agreement to the nearest tdc bin (0.25 nanosecond per bin).

The cloud muon peak (Gaussian in shape) has a FWHM $\sim$ 10 nanoseconds and at 29.8 MeV/c it is estimated to be centered at 35.0 ns in the TOF spectrum for one RF cycle in Figure 4.14(a). Thus most of the cloud muons ($\sim$96 %) are in the first bin and the remaining appear in the 6th bin.

4.8.3 Positron Suppression

The pulse height cut applied on the C_{in} counter suppresses the positron background from $\sim$1 positron per surface muon to $\sim$ 0.004 positron per surface muon at 29.8 MeV/c. Figure 4.13(b) indicates the remnant positrons in the time of flight spectrum at 33.1 MeV/c when the pulse height cut is applied. This momentum is chosen as an illustration because the cloud muon peaks are arriving far behind the beam positrons. About 55 % of the remnant positrons are beam positrons and they do not move across the TOF spectrum when the beam momentum changes.

It is important to calculate this unwanted background in the six bins of the RF period in order to understand the variation in the polarization of the muon beam across the RF cycle.

4.8.4 Asymmetry Variation

It was found that the polarization of the beam is maximum at the $\mu - \pi$ edge. Since the contaminant π^+'s, cloud μ^+'s and beam e^+'s are strongly time correlated with respect to the RF it would be worthwhile to investigate how the polarization of the beam varies across one cyclotron period.

The mechanism described in Chapter two produces muons that are intrinsically close to being 100% polarized. However in a real experiment there are depolarization effects; and in this beam test there are three contributions:

- The muon beam divergence is not zero and thus the polarization is decreased by a factor given by the average of cos θ, where θ is the angle of the muon's momentum vector with respect to the beam axis.

- A typical positron detector intercepts a rather large solid angle and thus averages appreciably over positron decay angles. For the upward and downward positron detectors in the detector setup shown in Figure 3.3,

$$\langle \cos\theta \rangle = \frac{\int_{-\theta'}^{\theta'} \cos\theta \; d\theta}{2\theta'} = 0.91,$$

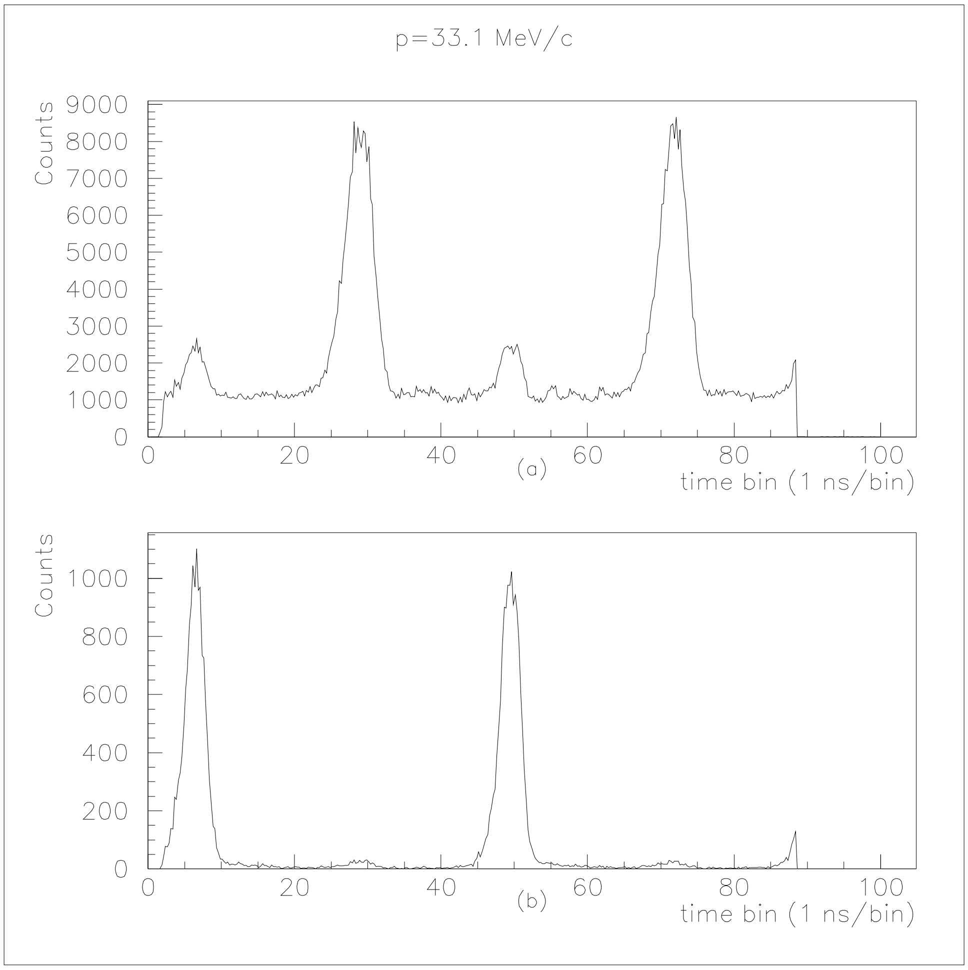

Figure 4.13: (a) Raw TOF, (b) TOF with pulse height cut, showing only cloud muons and remnant positrons.

where $2\theta'$ is the angle subtended at the aluminum target by the two positron detectors and $\theta' = \tan^{-1}\frac{3.25}{3.75}$, assuming the target position is centered with respect to the detectors. This smears the decay distribution, resulting in an apparent depolarization of 9±2% . The error of ±2% is due the uncertainty in the position and geometry of the counters.

- The depolarization effect of multiple scattering of muon passing through matter is negligible. At $\triangle$p/p = $\frac{1}{2}$ %, $\langle\cos\,\theta\rangle$=0.9999 for carbon target. Multiple scattering of the nonrelativistic muons from pion decay at rest changes the muon's direction of motion without changing its spin direction.

The asymmetry for the muon decay in the six different bins of the cyclotron period is calculated by applying the fitting equation (4.1) to the positron spectra of the upward counter corresponding to the different time bins. Two cuts are applied to the these spectra:

- A dE/dx cut on the pulse height distribution in the C_{in} counter (ADC3 $>$ 250).
- No pile-up muon present (TDC8 $<$ 100).

The asymmetry fits are shown in Figure 4.15 and the polarization versus bin number is plotted in Figure 4.14(b). The polarization incorporates the correction for the the finite angle effect of the positron counter, and the error bars are mostly due to the systematic uncertainty in the geometry of the counter. The following four points are noted from Figure 4.14(b):

- As explained in the previous section, the unwanted particles have a higher flux in the first and last bins; the cloud μ^+'s in the first and the e^+'s in the sixth bin.

Results at 29.8 MeV/c (flux in counts/(μA sec))			
time bin #	**backgr flux**	**(surface μ^++backgr) flux**	f_μ
1	0.258 ± 0.001	1.31 ± 0.04	0.80 ± 0.04
2	0.007 ± 0.001	0.87 ± 0.02	0.99 ± 0.04
3	0.0030 ± 0.0002	1.10 ± 0.03	1.00 ± 0.04
4	0.0019 ± 0.0001	1.49 ± 0.04	1.00 ± 0.05
5	0.0030 ± 0.0002	1.95 ± 0.06	1.00 ± 0.06
6	0.018 ± 0.001	2.57 ± 0.07	0.99 ± 0.06

Table 4.4: The background comprises remnant positrons and cloud muons, $f_\mu =$ surface μ^+/(surface μ^+ + background). The cyclotron period is divided into six bins of 7.25 nanoseconds.

- The polarization is lowest in the first bin because of the lowest surface muon to background ratio.

- The polarization rises from the first to the fifth bin because of the exponential fall with time in the surface muon flux from pion decay at rest (the horizontal axis goes backward in time) and the consequent relative decrease in the background contribution.

- The polarization drops in the sixth bin due to the fall in the surface muon to background ratio, the remnant beam positrons is highest in this bin.

The background flux, the surface muon flux and the ratio f_μ of surface muon flux to sum of surface muon and background flux are calculated in the six bins of the time of flight spectrum at 29.8 MeV/c (Figure 4.14 (a)) in the Table 4.4.

Since the background comprises cloud muons and accidental positron coincidences which are randomly polarized and have no asymmetry, it is expected that f_μ should agree with the ratio of asymmetry of the clean surface muon beam to

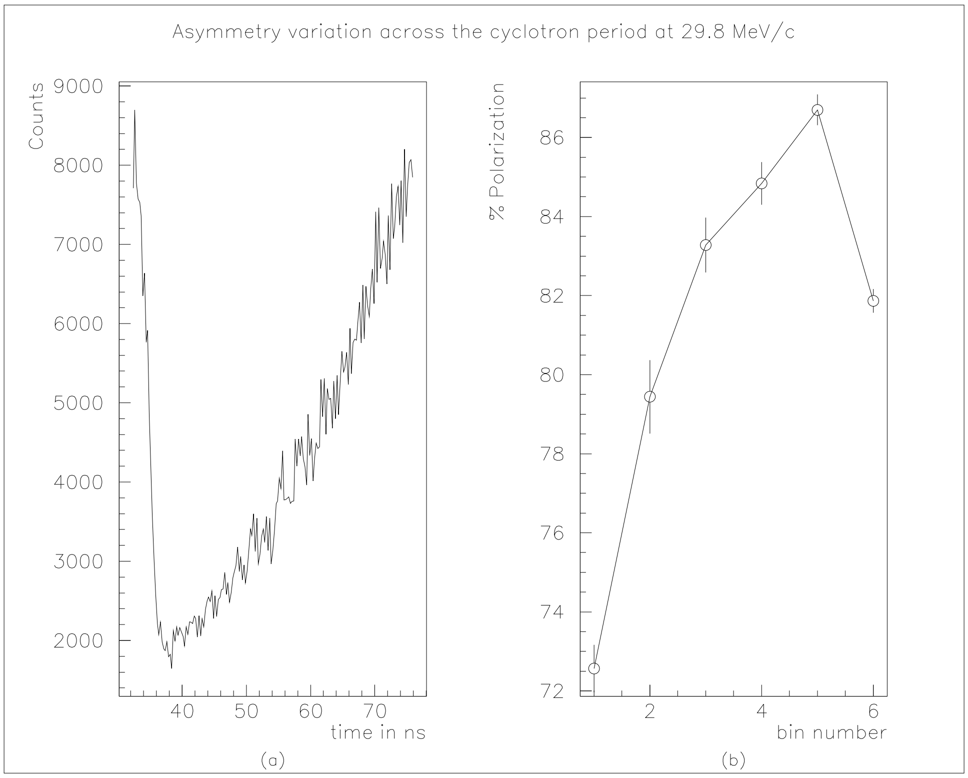

Figure 4.14: (a) The TOF spectrum for one RF cycle from 32.5 ns to 76.0 ns with ADC cut (to suppress the e^+), and (b) The polarization of the surface μ^+'s in the six bins (7.25 ns per bin) into which the TOF spectrum in (a) was divided.

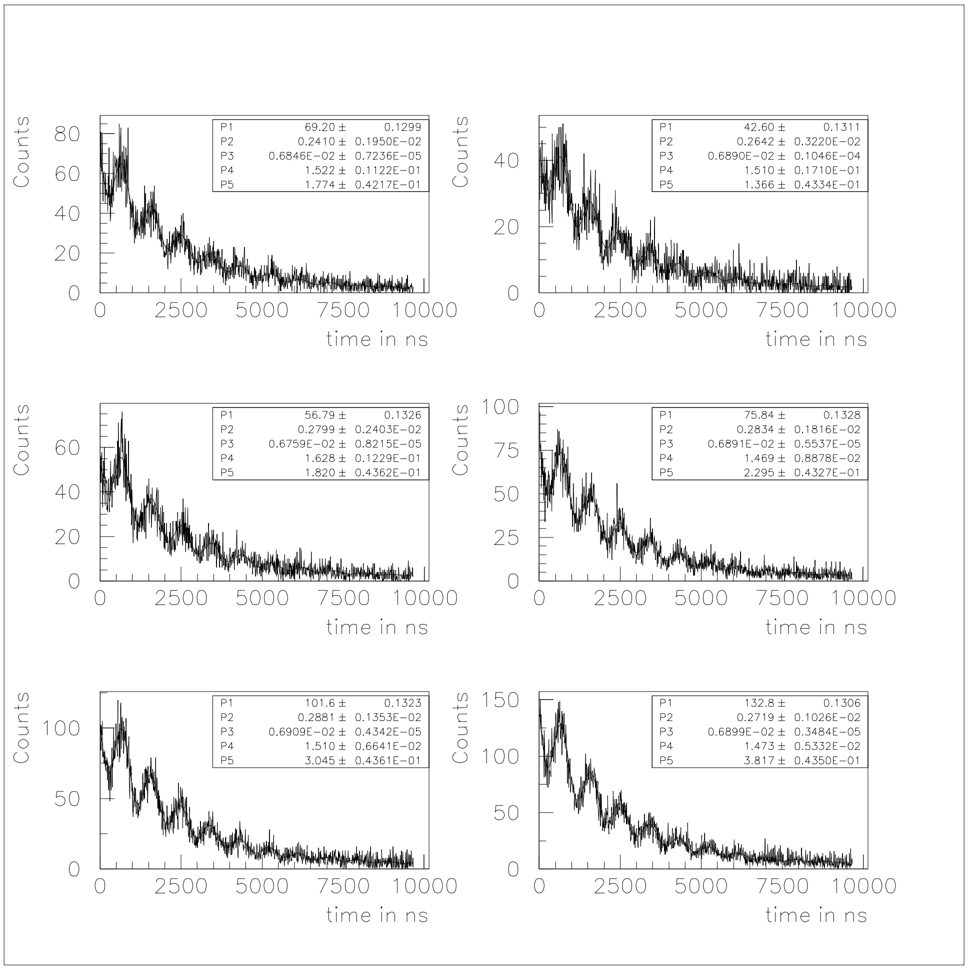

Figure 4.15: Fitting parameters at 29.79 MeV/c for muon decay in the six time bins. Cuts were applied on e^+'s, and pile-up μ^+'s. P1$\equiv$ N_0, P2$\equiv$ α, P3$\equiv$ ω, P4$\equiv$ ϕ, P5$\equiv$ Bkg.

Asymmetry results at 29.8 MeV/c		
Bin number	**measured α**	α/f_μ
1	0.2410 ± 0.0020	0.30 ± 0.02
2	0.2642 ± 0.0032	0.27 ± 0.01
3	0.2799 ± 0.0024	0.28 ± 0.01
4	0.2834 ± 0.0018	0.28 ± 0.02
5	0.2881 ± 0.0014	0.29 ± 0.02
6	0.2719 ± 0.0010	0.27 ± 0.02

Table 4.5: α/f_μ = calculated asymmetry of clean surface μ^+ beam in M11.

that of the surface muon beam with the remnant background. From the discussion above on depolarization effects the asymmetry of the clean surface muon beam in M11 is estimated to be ~ 0.28. This value can be tested by measuring the ratio α/f_μ, where α is the measured asymmetry in the different bins. If the background is understood correctly, the quantity $\alpha/f_\mu \simeq 0.28$, independent of the tdc bin. This is approximately the case, as shown in Table 4.5.

4.9 Time Window Selection

For positrons suppression pulse height selection was used. As for cloud muons and pions, one way to avoid them is to select a time window in the TOF spectrum in which cloud μ^+ peak is excluded. Moreover the time window can be selected to exclude the remanant beam positrons so that the overall positron contamination is ~ 0.3 % of the total surface muon beam flux.

An acceptance region from 45.0 ns to 71.3 ns was chosen from the time of flight at a momentum of 29.8 MeV/c. A combination of the cut based on this and the one from pulse height shape of C_{in} (i.e. ADC3 greater than 250) increases the

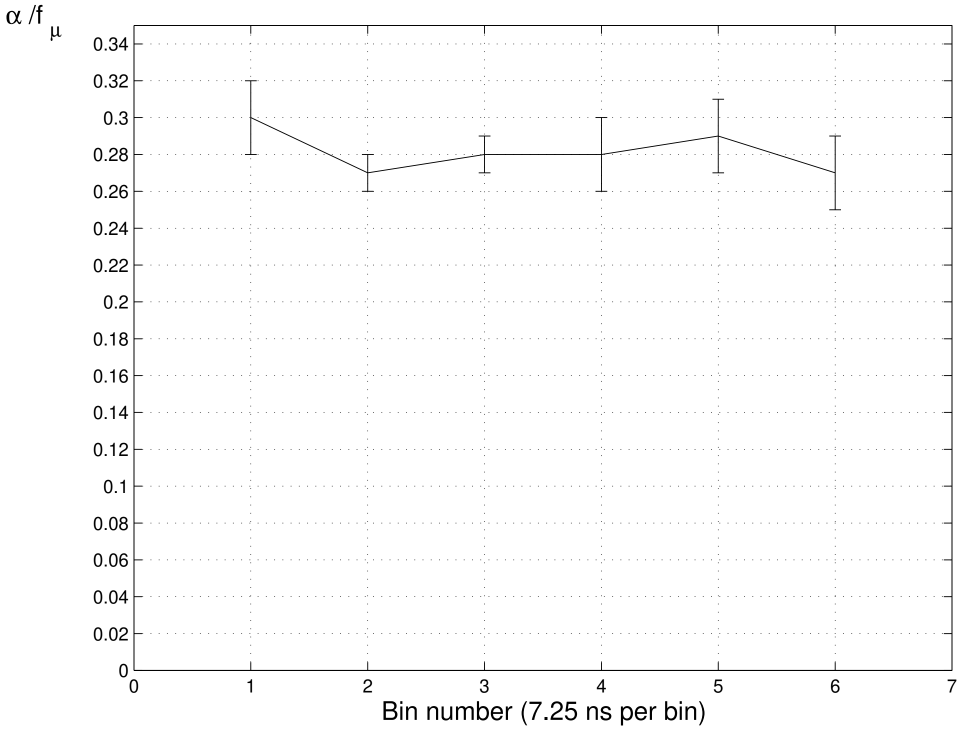

Figure 4.16: Graph of α/f_{μ} versus Bin number

Asymmetry at the $\mu - \pi$ edge (29.8 MeV/c)		
Selection	**asymmetry**	**Polarization**
No cuts	0.2278±0.0001	
pulse height cut	0.2682±0.0001	(88.4±2.0)%
pulse height and TOF cuts	0.2852±0.0005	(94.0±2.2)%
pulse height, TOF and pile-up-gate cuts	0.2849±0.0005	(93.9±2.2)%

Table 4.6: Selections to optimize the asymmetry at 29.8 MeV/c. The polarization incorporates the correction for the finite angle effect of the positron counter.

asymmetry from 0.228 to 0.285, see Table 4.6. Figure 4.17 shows the fit for the asymmetry. A further cut on the pile-up-gate to suppress pile-up muons leaves the asymmetry almost unchanged (Figure 4.18).

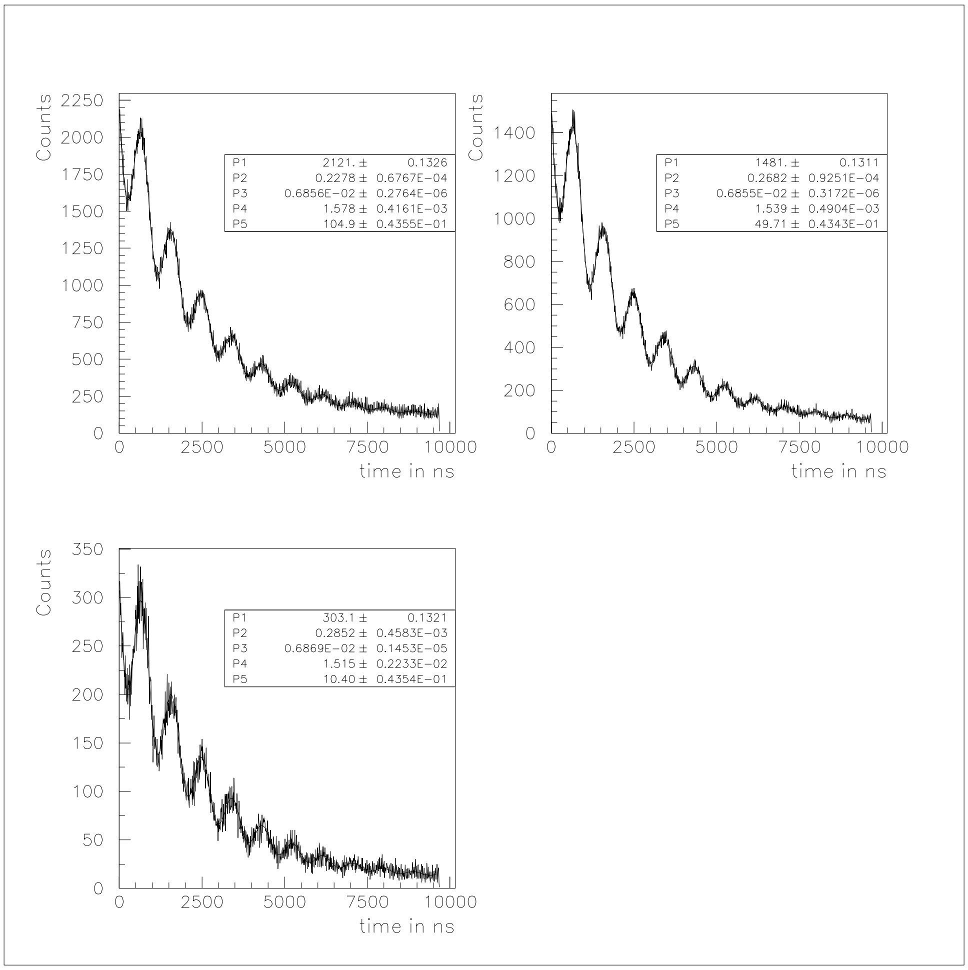

Figure 4.17: Asymmetry fits with no cuts (α=0.228), with adc cut only (α=0.268), with both time and adc cuts (α=0.285) at the $\mu - \pi$ edge. Only the upward positron counter is considered.

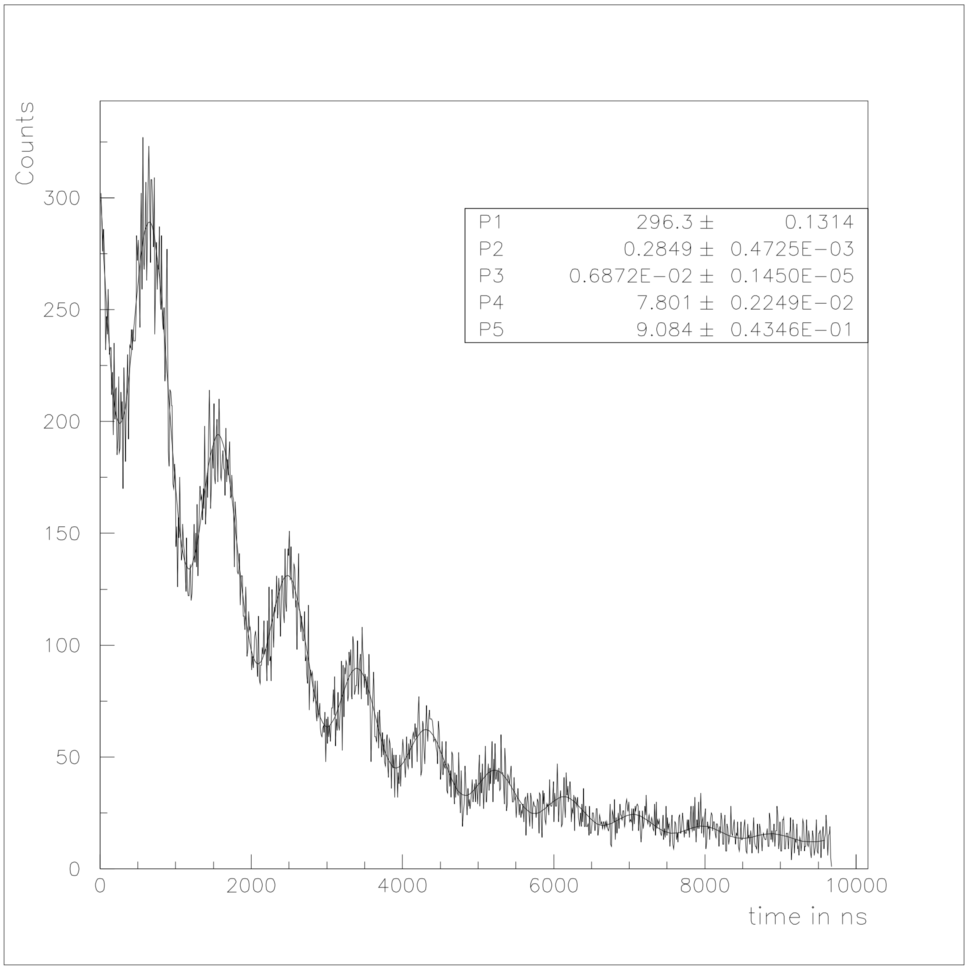

Figure 4.18: Asymmetry fits with pile-up-gate cut, time and adc cuts (α=0.285) at the $\mu - \pi$ edge. Only the upward positron counter is considered.

Chapter 5

CONCLUSION

The secondary beamline M11, known as a fast pion channel, of the 500 MeV cyclotron at TRIUMF was tested to investigate its use as a surface muon source. It was run at momenta ranging from a few % above and a few % below 30 MeV/c. The correspondig low velocity of $\sim$4 MeV muons from pion decays at rest makes it possible to achieve excellent identification of muons with thin scintillation counters and electronic logic. Leaving the production target the beam consists of pions, muons and positrons.

A detailed analysis was done at 29.79 MeV/c (the $\mu - \pi$ edge), the momentum of surface muon from pion decay at rest in the 1AT1 production target. At this momentum the maximum surface μ^+'s flux measured on M11 is 9.5 $\pm$ 0.3 counts/μA sec, after suppression of positrons and pile-up muons. These surface μ^+'s have a polarization of 88.4$\pm$2.0%. The depolarization of $\sim$12% is mainly due to

- the non-zero μ^+ beam divergence,
- pions and cloud muons (which is 2.7% of the surface μ^+ flux) and
- remnant positrons (which is 0.4% of the surface μ^+ flux) .

At the $\mu - \pi$ edge (29.8 MeV/c)	
Particle	**Flux in counts/μA sec**
surface μ^+	9.46±0.33
cloud μ^+	0.26±0.02
beam e^+	>6.0±0.2
decay e^+	>3.7± 0.3
π^+	$\sim$ 0.018±0.001

Table 5.1: The flux of the different particles at 29.8 MeV/c. No time cut is applied for these data.

A time window was selected from the 43.5 nanosecond RF period to suppress the beam positrons, the cloud muons and pions. It is found that the three unwanted particles are time correlated with the RF and arrive close together in time in an interval of 21 nanoseconds. Since there are surface muons at all times during the cycle, a time window selection of 26.3 ns reduces the surface μ^+ flux to 1.94 $\pm$ 0.07 counts/μA sec. The polarization increases to 93.9±2.2%. This time cut together with the ADC cut and the pile-up-gate cut reduced the background (positron contamination) to $\leq$ 0.7% of the surface muon flux. It was verified that the cloud μ^+'s do not have any asymmetry, i.e. they are not polarized. The pion flux is very small and is excluded in the time window selected.

The flux result at the $\mu - \pi$ edge (29.8 MeV/c) is shown above in Table 5.1. The decay positrons has a flat distribution in time. The value given for the pion flux is an approximation since it is actually the pion flux at 33.1 MeV/c.

To conclude, this beam test has increased our understanding of the M11 at the transition momentum 29.8 MeV/c where the surface muon flux is at its maximum and then drops to zero.

Bibliography

[1] C.Caso *et al.*, The European Physical Journal **C3** (1998) 1.

[2] A. E. Pifer, T. Bowen, and K. R. Kendall, Nucl. Instrum. Methods **135**, 39, (1976).

[3] T. Bowen, Physics Today **38**, 22 (July 1985).

[4] T. D. Lee and C. N. Yang, Phys. Rev. **104**, 254 (1956)

[5] C. S. Wu *et al.*, Phys. Rev. **105**, 1413 (1957).

[6] R. L. Garwin, L. M. Lederman and M Weinrich, Phys. Rev. **105**, 1415 (1957).

[7] L. Michel, Proc. Phys. Soc. **A63**, 514 (1950).

[8] M. L. Brooks *et al.*, Phys. Rev. Lett. **83**, 1521 (1999).

[9] TRIUMF Users Handbook, 1987.

[10] S. F. G. Cox, J. Phys. C **20**, 3187 (1987).

[11] A. Amato, Rev. Mod. Phys. **69**(4), 1124 (1997).

[12] D.Fleming and M Senba in: Prespective of Meson Science, Chapter 8, eds. T. Yamazaki, K. Nakai and K. Nagamine (Elsevier Science Publishers B.V. 1992).

[13] K. W. Kehr,D. Richter, and J. -M. Welter, Phys. Rev. B **26**(2), 567 (1982).

[14] TRIUMF Data Aquisition Systems Group web repository, VDACS Data Aquisition System.

[15] P. W. Green, NOVA Data Analysis System, Version 2.0, 1995.

[16] T.Numao *et al.*, Phys. Rev. D **52**, 4855 (1995).

[17] C. J. Oram *et al.*, Nucl. Instrum. Methods **179** , 95 (1981) .